Isabelle C.P. van Dongen

A finite element model to determine the bactericidal and cytotoxic properties of nanopatterned surfaces:

A parametric study



A finite element model to determine the bactericidal and cytotoxic properties of nanopatterned surfaces:

A parametric study

By

Isabelle van Dongen

in partial fulfilment of the requirements for the degree of

Master of Science

in Biomedical Engineering

at the Delft University of Technology

to be defended publicly on Tuesday December 12, 2017 at 11:30 AM

Supervisors: Dr. Saber Amin Yavari TU Delft / UMC Utrecht

Mr. Mohammad J. Mirzaali TU Delft

Prof. Dr. Harrie Weinans TU Delft / UMC Utrecht

Prof. Dr. Amir A. Zadpoor TU Delft

Exam Committee: Prof. Dr. Amir A. Zadpoor TU Delft

Dr. Saber Amin Yavari TU Delft / UMC Utrecht

Dr. Lidy-Fratila-Apachitei TU Delft Mr. Mohammad J. Mirzaali TU Delft Dr. Timon Idema TU Delft





Preface

One of the requirements for the master Biomedical Engineering at the Technical University in Delft is an internship. From September 2016, I spend 3 months in Bologna, Italy, at the Rizzoli Orthopaedic Institute at the Laboratory of Immunorheumatology and Tissue Regeneration. In these 3 months I have seen a lot of laboratory work and learnt a lot about tissue regeneration. I have met a lot of wonderful people working at the Rizzoli who tried to learn me all about tissue regeneration.

Once I came back to the Netherlands, I wanted to start my thesis project for the master Biomedical Engineering. I preferred to work at a laboratory, like I had seen in the Rizzoli Institute. I contacted Prof. Dr. Harrie Weinans, with whom I already was in contact for my internship. He introduced me to the University Medical Centre Utrecht, where I could start my thesis project at the department of Orthopaedics. My daily supervisor was Dr. Saber Amin Yavari. Dr. Saber Amin Yavari introduced me to the project about layer-by-layer coatings on implants. An interesting surface modification technique for the prevention of implant-associate infection. I started working on my literature study and I read a lot about nanopatterning, another surface modification technique. I talked to Dr. Saber Amin Yavari, and we decided to shift the focus of my project to nanopatterning. In combination with the Technical University of Delft, the idea of modelling the interaction of nanopatterned surfaces with bacterial cells and host cells came up. Prof. Dr. Amir Zadpoor and Mr. Mohammad Mirzaali guided me to further finalise the idea by using a Finite Element Model. In close collaboration with Dr. Saber Amin Yavari and Mr. Mohammad Mirzaali we modelled the interaction between the nanopatterned surface and host cells, where you will further read about in my thesis.

I would like to use this opportunity to express my gratitude towards all my supervisors. First of all, I would like to thank Dr. Saber Amin Yavari for guiding and encouraging me throughout the process and giving me the opportunity to come up with new ideas for the project. I would like to thank my second supervisor, Mr. Mohammad Mirzaali, who helped me during the modelling phase of my project and from whom I learned a lot of modelling skills. Also, I would like to thank Nazli Sarkalkan, who helped me with the modelling as well. I would like to thank Prof. Dr. Harrie Weinans, who guided me at the beginning of my thesis project and offered me an opportunity to work at the University Medical Centre in Utrecht. I would like to give a special gratitude to my supervisor and coordinator of my specialisation, tissue biomechanics and implants, Prof. Dr. Amir Zadpoor, for giving me the opportunity to adjust my project and providing a work space for me making sure I could continue with the project.

Besides my supervisors, I would like to thank my family and friends. Especially my father and mother, who gave me the opportunity to start studying after high school and who were always there for me. They even helped me moving six times during my study in a time period of less than six years. At last, I would like to thank Hessel Kruk for always supporting me.

Isabelle C.P. van Dongen Utrecht, November 30, 2017

Abstract

The fundamentals of the nanopatterned surface can be found on the wings of cicada. These bactericidal surfaces are artificially mimicked on the surface of the implant to reduce the infection rate, which is one of the main complication after joint replacement. The bactericidal properties of the nanopatterned surface are a promising feature. However, the non-cytotoxicity of the surface of the implants should not be compromised. So far, no optimal nanopatterned surface regarding the geometrical features has been found yet. This study focusses on the computational modeling of the nanopatterned surface using Finite Element approaches to simulate the interaction between bacterial cells (Staphylococcus aureus) and host cells (osteoblast) with the nanopatterned surface. The final aim of the project is to show how geometrical features of the nanopatterned surfaces can influence the bacteria's and cell's fate. The geometrical parameters of the nanopatterned surface are height, width, interspace, radius and the shape and are varied to create different types of nanopatterned surfaces. The simulations have been performed based on the experimental examination of the bactericidal and cytotoxicity properties of nanopatterned surfaces. From the numerical analysis, it is concluded that among different geometrical parameters of the nanopatterned surface, only width and interspace of the nanopillars have a direct bactericidal effect. The nanopatterned surface with a small/intermediate width (50 nm) in combination with a large interspace (300 nm) has been found as the most optimal nanopattern resulting in bactericidal properties and non-cytotoxic properties for host cells. The results of this project can be considered as a guideline for the proper design of geometry of nanopatterned surfaces and can be verified by further experimental investigations.

Table of content

1.	. Introduction	1
	1.1 Staphylococcus Aureus	2
	1.2 Osteoblast cell	3
2.	. Methods	
	2.1 Staphylococcus Aureus	
	2.1.1 Geometry	
	2.1.2 Material properties	5
	2.2 Osteoblast cell	7
	2.2.1 Geometry	7
	2.2.2 Material properties	8
	2.3 Nanopatterned surfaces	8
	2.3.1 Geometry	8
	2.3.2 Material properties	9
	2.4 Finite Element simulation	9
	2.4.1 Meshing	10
	2.4.1.1 Interaction of the Staphylococcus aureus with the nanopatterned surface	10
	2.4.1.2 Interaction of the osteoblast with the nanopatterned surface	10
	2.4.2 Loading, boundary conditions and interaction	10
	2.4.2.1 Loading of Staphylococcus aureus	12
	2.4.2.2 Osteoblast cell	12
	2.4.3 Simulation setup	13
	2.5 Statistical analysis	16
3.	. Results	17
	3.1 Parametric study	17
	3.1.1 Height	17
	3.1.2 Interspace	19
	3.1.3 Width	21
	3.1.4 Radius	22
	3.1.5 Shape	24
	3.2 Von-mises strain criterion for the rupture detection of cells	25
	3.2.1 Bactericidal effects	26
	3.2.2 Cytotoxic determination of host cells	27
	3.3 Statistical models	

3.3.1 Correlation between maximum strain and sinking depth	30
3.3.2 ANOVA-test	31
3.3.3 Correlation between the maximum strain and the ratio of width and interspace	32
3.3.4 Correlation between the maximum strain and the ratio of radius and interspace .	33
4. Discussion	2/
4.1 Effects of geometrical features of nanopatterned surface on the host cells and	54
bacteria's fate	34
4.2 Suggestion for the improvement of the FE simulations	37
4.2.1 Difficulties of the FE simulation	37
4.2. Potential validation of the model	37
4.2.3 Future research	38
4.2.3.1 Experimentally validation of the FE model	38
4.2.3.2 Increasing the complexity of the FE model	39
4.2.3.3 Another mechanism to describe the mechanism of the nanopatterned surface	
4.2.3.4 Elaboration of the concept of nanopatterned surface to other research fields	.40
5. Conclusion	42
6. Supplementary information	43
6.1 Analysis of the time period	43
6.2 Analysis of the ratio of the Young's modulus	43
6.3 Mesh refinement	44
6.3.1 Meshing of Staphylococcus aureus	44
6.3.2 Meshing of the osteoblast cell	45
6.4 Interaction between the cytoplasm and the cell wall of Staphylococcus aureus	46
6.5 Analysis of the hyperelastic coefficients	47
7. Bibliography	49

1. Introduction

In nature, nanostructures are found on the wings of cicada and dragonfly. The nanostructures have a pillar shape and possess an antibacterial mechanism. When bacteria adhere to the surface of the wings, the mass of the wings will increase, obstructing the insects to fly (Ivanova et al., 2012). The pillars can directly penetrate the bacterial wall or stretch the bacterial wall. When the stretching of the bacterial wall becomes too high, cracks will be formed in the bacterial membrane resulting in leakage of the cytoplasm out the bacteria. That causes the bacteria to rupture (Bandara et al., 2017). An experimental study of Kelleher et al. (2015) shows that the nanopillared surface of cicada has an bactericidal effect due to the rupturing of bacteria (Figure 1). The nanopillars found on the wings of cicada have a height of 200 nm, an interspace between the pillars of 170 nm, a width at the base of 100 nm, and a width at the cap of 60 nm (Elbourne et al., 2017). The nanopillars found on the wings of dragonfly show small and tall pillars. The small pillars have a height of 189 nm and a width of 37 nm, while the tall nanopillars have a height of 311 nm and a width of 57 nm (Bandara et al., 2017).

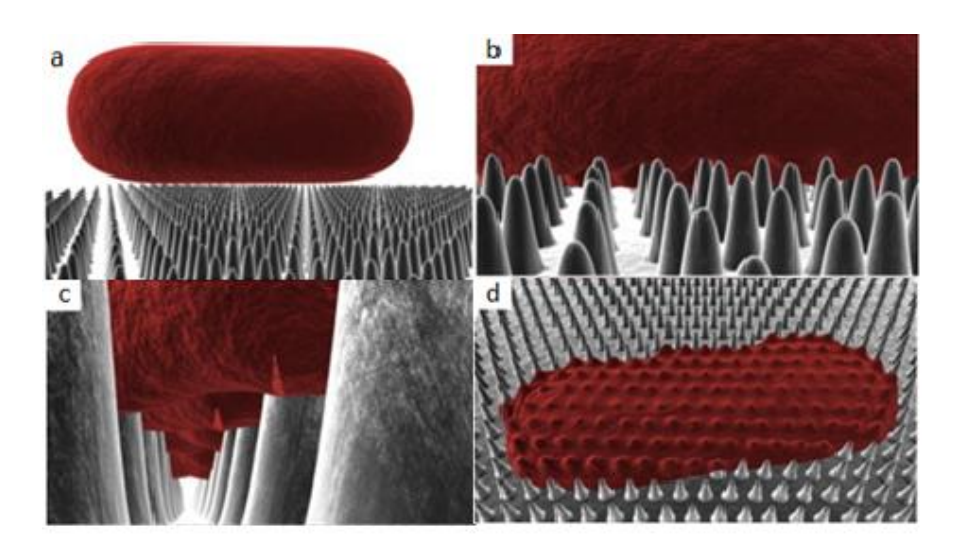


Figure 1: Mechanistic explanation of bactericidal activity of a nanostructure (Pogodin et al., 2013).

These bactericidal properties of the nanopatterned surface are a promising feature for the orthopaedic field. In the orthopaedic field, implant-associate infections are the main complication. Infections are due to the adherence of bacteria to the surface of the implant. Joint replacements result in 0.5 - 5% of the cases in infection (Campoccia et al., 2006). After implantation, the defense system of the human body becomes weaker. The concentration of bacteria needed to evoke an infection is decreased by a factor of 100.000, so bacteria induce more easily infections after implantation (Kapadia et al., 2016).

The concept found on the wings of dragonfly and cicada may help to lower the infection problem. The nanopatterned surface can be artificially mimicked on the surface of the implant. The bactericidal effect of the nanopattern can prevent the attachment of bacteria to the surface of the implant. Dickson et al. (2015) created nanopillars using nanoimprint lithography as a fabrication method. The nanopillared surface showed a higher bactericidal effect than flat surfaces (Dickson et al., 2015). Also, Diu et al. (2014) created a nanostructured surface consisting of nanowires based on hydrothermal treatment. This nanowired surface resulted in a selective bactericidal effect and no cytotoxic effect for host cells (Diu et al., 2014). The nanostructured surface of Hasan et al. (2015) consisted of nanopillars based on deep reactive ion etching and showed cytotoxic properties against bacteria and against host cells (Hasan et

al., 2015), in contrary to the study of Diu et al. (2014). Cytotoxic host cells can result in a lack of osseointegration leading to an unstable joint. It is important the nanostructure does not show cytotoxic properties against host cells.

A lot of different parameters affect the interaction between cells and the nanopatterned surface. Size, shape, and density of the nanopattern can influence the fate of the cells. While cell type (e.g., fibroblast, osteoblast, gram-positive bacteria or gram negative-bacteria) influences the efficacy of the mechanism of the nanopatterned surface. It is a challenge to find an optimal geometrical design for the nanopatterned surface resulting in desired outcomes (Tripathy et al., 2017). Finding a nanopatterned surface with optimized geometrical features resulting in the killing of bacteria, while being non-cytotoxic to host cells would be ideal. Some correlations between the geometry of the nanopatterned surface and the bactericidal properties already exist in the literature (Li, 2016; Tripathy et al., 2017; Xue et al., 2015). It has been found that the sharper the nanopillars, the higher the achieved bactericidal properties (Xue et al., 2015). Also, a smaller width of the nanopillar results in a higher bactericidal effect of the nanopatterned surface (Tripathy et al., 2017). Xue et al. (2015) have found that a more substantial interspace between the pillars results in higher bactericidal properties. This is in contradictions with the findings of Kelleher et al. (2015), showing that a smaller interspace results in higher bactericidal properties. Li (2016) shows analytically that a more extensive height results in higher bactericidal properties. However, other studies have shown no change in bactericidal properties based on varying the height (Tripathy et al., 2017). These contradictions make it challenging to find the exact correlation between the geometrical features of the nanopattern and its effect on bacteria's fate.

Finite element (FE) modeling can be used to examine the interaction between bacteria and nanopatterned surfaces. The nanopatterned surface can be modeled using different types of shapes and different geometrical parameters. Variation of the shape and the geometrical parameters can give more insight into an optimized nanopatterned surface regarding the killing efficacy of bacteria. Furthermore, the optimized nanopatterned surface should be non-cytotoxic for host cells. In this study, within various non-linear parametric numerical simulations, the interaction of bacteria and osteoblast cells with the nanopatterned surface with different geometrical features has been investigated. Bactericidal properties have been measured based on strain-based criterion implemented on FE results.

1.1 Staphylococcus Aureus

The simulated bacteria is the Staphylococcus aureus (Figure 2). Staphylococcus aureus is a common bacteria in the human body and can cause bone and joint infections (Lowy, 1998). This gram-positive bacteria has a circular shape and a relatively thick cell wall consisting of peptidoglycans. The function of the bacterial wall is to protect the integrity of the interior of the cell due to its strong outer layer and to give the bacteria its shape (Bailey et al., 2014; Shockman and Barren, 1983). The peptidoglycans in the wall give the bacterial wall its mechanical strength. Due to the thick membrane, the mechanical strength of Staphylococcus aureus is relatively higher than other bacteria such as Escherichia coli (Xue et al., 2015). The cell wall of the bacteria encloses the cytoplasm. The cytoplasm is a water-like substance containing organelles which perform internal processes (e.g., protein synthesis and DNA replication) (Bailey et al., 2014).

The rupture of Staphylococcus aureus is determined based on a strain-dependent threshold. If the maximum strain in the bacterial wall of Staphylococcus aureus exceeds this threshold, the bacterial wall will break. As already explained, breakage of the bacterial wall leads to apoptosis of the bacteria (Bandara et al., 2017). In the article of Thwaites and Mendelson (1985) a bacterial thread resembling a gram-positive bacteria, has been tested to determine its mechanical properties. The bacterial thread breaks at a rupture strain of 0.5.

1.2 Osteoblast cell

The simulated host cell is the osteoblast cell. Osteoblasts are responsible for new bone formation and are aiding the osseointegration process (Craig et al., 2015). Osseointegration refers to the direct bone-to-implant interface without the interposition of non-bone tissue (Mavrogenis et al., 2009). A lack of osseointegration can cause implant failure. Therefore, it is essential the nanopatterned surface is non-cytotoxic for the osteoblast cells.

The rupturing of the osteoblast cell is also determined based on a strain-dependent threshold. In the article of Li et al. (2013) the membrane of an erythrocyte has been tested. The plasma membrane of the osteoblast cell consists of a lipid bilayer (Wang and Anslyn, 2011), just like the membrane of the erythrocyte cell (Li and Lykotrafitis, 2014). The rupture strain of the cell wall is 1.05.

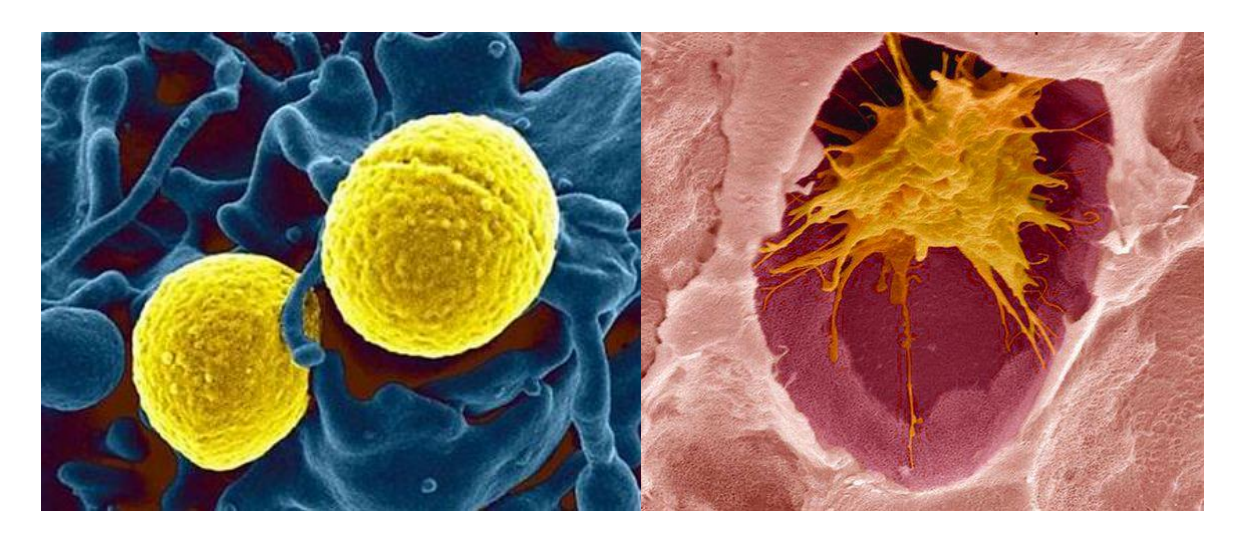


Figure 2: Visualisation of the bacteria Staphylococcus aureus (a) and the osteoblast cell (b).

This study will focus on the effect of nanopatterned surfaces on Staphylococcus aureus and osteoblast cells, using a FE model. Height, interspace, width, radius and sharpness of the nanopatterned surface will be varied. By variating these five parameters, the effect of the geometrical features of the nanopatterned surface on the behaviour of both cells will be tested. The bactericidal and cytotoxic properties will be calculated for every simulation. The most optimized nanopatterned surface will be the nanopattern with the highest bactericidal properties and the lowest cytotoxic properties.

2. Methods

The interaction between the nanopatterned surface and cells was simulated based on the experimental examination of the nanopatterned surface with bacteria or host cells, performed in the study of Hasan et al. (2015) and Dickson et al. (2015). When the nanopatterned surface was experimentally tested, first the nanopatterned surface had to be fabricated. Different fabrication methods could be used: nanoimprint lithography, anodizing or electrodeposition (Dickson et al., 2015; Wu et al., 2016). The fabricated nanopatterned surface was put into a culture well plate for examination (Hasan et al., 2015). For the bactericidal tests, the bacterial cells were dissolved in a medium (Dickson et al., 2015). For cytotoxicity tests, the host cells were dissolved in the medium (Hasan et al., 2015). Both mediums were individually disposed on top of the nanopatterned surface. Dependent on the experimental set up of the study, the cells were analysed after a particular incubation time, ranging from 1 – 18 hours (Diu et al., 2014; Ivanova et al., 2012). This research simulated the experimental examination of the interaction of Staphylococcus aureus and an osteoblast cell with the nanopatterned surface. The simulation was performed with a Finite Element software: ABAQUS/CAE Version 6.14 (© Dassault Systèmes, 2014).

First, the interaction of the nanopatterned surface and the bacteria was simulated. The bactericidal properties were determined based on the maximum strain in the bacterial wall. Twenty-two different types of nanopatterned surfaces (Table 11) were modelled and their effect on Staphylococcus aureus was examined. The four best performing nanopatterned surfaces (Table 11) were chosen for the simulations with the osteoblast cell. The best performing nanopatterned surfaces were determined based on the highest maximum strain in the bacterial wall. If the maximum strain in the bacterial wall exceeded the strain criterion, the nanopatterned surface caused a rupture in the bacterial wall. Secondly, the simulations of the nanopatterned surface and its interaction with host cells were evaluated. The nanopatterned surface is non-cytotoxic if the strain in the cell wall of the osteoblast cell did not exceed the threshold criterion for rupturing of osteoblast cells.

In the next section, the geometry and the material properties of Staphylococcus aureus, the osteoblast cell and the nanopatterned surface will be determined. Followed by the description of the meshing, loading, boundary conditions and interaction, and the simulation setup of the FE simulation. Then the statistical analysis is explained.

2.1 Staphylococcus Aureus

Staphylococcus aureus and the osteoblast cell belonged to different size scales. The size of bacterial cells was on the nanoscale. Some distinctive characteristics of Staphylococcus aureus were its thick cell wall, mainly consisting of peptidoglycan (Shockman and Barren, 1983) and that Staphylococcus aureus was a prokaryotic cell (Milner et al., 2012).

2.1.1 Geometry

Staphylococcus aureus was modelled consisting of cytoplasm and a cell wall. Constituents such as organelles inside the cytoplasm and the polymers inside the bacterial wall were neglected. The shape of Staphylococcus aureus was circular. The outer diameter of the bacterial cell was 600 nm (Eaton et al., 2008). The bacterial wall had a thickness of 10 nm (Table 1) (Figure 3) (Pogodin et al., 2013).

Table 1: Geometrical features of Staphylococcus aureus.

	Cytoplasm	Cell wall
Shape	Circular	Circular
Maximum diameter (nm)	580	N/A
Thickness (nm)	N/A	10

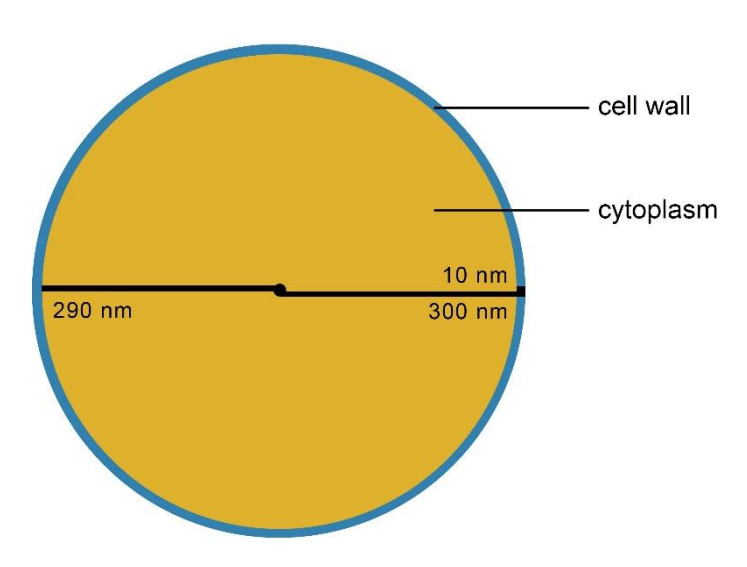


Figure 3: The geometric features of Staphylococcus aureus: the cytoplasm and the cell wall.

2.1.2 Material properties

As explained before, Staphylococcus aureus was modelled consisting of cytoplasm and a bacterial wall. The material properties of both parts were different. The cytoplasm had viscoelastic properties (Hartmann et al., 2006), while the bacterial wall had elastic properties (Xue et al., 2015). Due to the lack of FE models of bacteria, it was difficult to obtain matching material properties. Since the properties of the cytoplasm of bacteria were similar to those of a chondrocyte (Zhou et al., 2005), these properties were used to simulate the cytoplasm of the bacteria. The viscoelastic properties were described by a standard linear viscoelastic solid model (Figure 6). Three parameters described the viscoelastic model: k1 (equilibrium modulus), k1+k2 (instantaneous modulus) and μ (bulk viscosity) (Table 4) (Trickey et al., 2000).

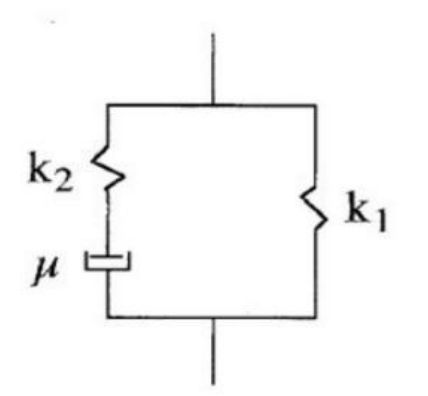


Figure 4: Standard linear viscoelastic solid model described by the equilibrium modulus (k1), the instantaneous modulus (k1+k2) and the apparent density (μ) .

Table 4: Parameters of the viscoelastic model describing the cytoplasm.

Properties of the viscoelastic model describing the cytoplasm

k₁ (KPa)	0.24
$k_1 + k_2 (KPa)$	0.41
μ (KPa*s)	3.1

For the implementation of a viscous elastic material into the FE model, a conversion from the properties of the cytoplasm into prony series had to be made. The following formulas calculated the shear modulus (g_1) and the time relaxation constant (τ) , which were the coefficients of the prony series (Zhou et al., 2005):

$$g_1 = \frac{k_2}{k_1 + k_2} \tag{1}$$

$$\tau = \frac{\mu}{k_2} \tag{2}$$

These coefficients of the prony series resembled the viscous behaviour of the cytoplasm and are listed in Table 5. The time relaxation constant (T) was the time needed for the model to fully adapt to the applied force (Zhou et al., 2005). In the FE model, a time period had to be implemented. The time period was dependent on the time relaxation constant. To make sure the simulation took into account the full relaxation, an analysis was performed of simulations with different time periods. These time periods were dependent on the time relaxation constant. The time periods longer than 187.5 seconds (281.25 seconds and 375 seconds) had an error percentage of 1% with respect to a time period of 187.5 seconds based on the outcome parameter of the average stress of a pillar. This low error percentage indicated that the simulation with a time period of 187.5 seconds took into account the full relaxation (S1).

The linear properties of the bacterial wall were modelled in the FE model as well. For the implementation of the linear material properties, a hyperelastic model was used. Hyperelastic models were often used as a substitution of linear models, especially in the models which resulted in a high elastic strain. The hyperelastic Neo-Hookean model showed the best approximation for linear elasticity (Zhou et al., 2005).

For the implementation of a hyperelastic material into an FE model, a conversion from the linear elastic properties into the Neo-Hookean coefficients had to be made. The Neo-Hookean coefficients (C_{10} and D_1) were calculated with the following formulas (Table 5) (Cowin and Doty, 2007):

$$C_{10} = \frac{\mu_0}{2} \tag{3}$$

$$D_1 = \frac{2}{K_0} \tag{4}$$

Where μ_0 was the initial shear modulus and K_0 was the initial bulk modulus. These two parameters could be calculated based on the following formulas:

$$\mu_0 = \frac{E}{2(1+v)} \tag{5}$$

$$K_0 = \frac{E}{3(1 - 2\nu)} \tag{6}$$

Where E was Young's modulus and v was the Poisson's ratio.

The bacterial wall consisted of elastic properties (Francius et al., 2008). The elastic properties of the bacterial wall were based on the computational model used in the study of Xue et al. (2015). The Young's modulus of the bacterial wall was 0.36 KPa and the Poisson's ratio was

0.45 (Xue et al., 2015). These parameters can be found in Table 5, as well as the visco- and hyperelastic coefficients for the cytoplasm.

Table 5: Coefficients of the material properties of the cytoplasm and the cell wall of Staphylococcus aureus.

Cytoplasm of Staphylococcus aureus		Cell wall of Staphylococcus aureus
Hyperelastic properties	Viscoelastic properties	Elastic properties
Neo Hookean coefficients Prony series		
$C_{10} = 6.21 * 10^5 MPa$	$g_1 = 0.39$	E = 6 KPa
$D_1 = 1666.7 \text{ MPa}^{-1}$	$k_1 = 0$	v = 0.45
	т = 18.75 s	

2.2 Osteoblast cell

A distinctive feature of the osteoblast cell was its size. The size of the osteoblast cell was on the microscale resulting in a much larger cell in comparison with Staphylococcus aureus which is on the nanoscale. Furthermore, another distinctive feature of the osteoblast cell was its existing nucleus (Milner et al., 2012).

2.2.1 Geometry

Osteoblast cells showed a typical polygonal morphology (Figure 2). Due to the complexity of the shape, a more straightforward shape of the osteoblast cell was used for the FE model. The geometry of the osteoblast cell for the simulation was the same as the geometry used in the article of Milner et al. (2012) and Wang et al. (2016). Milner et al. (2012) used a hat shape for the cytoplasm of the osteoblast and an ellipse shape for the nucleus. The cell wall followed the shape of the cytoplasm (Wang et al., 2016). The maximum horizontal diameter of the cytoplasm was 20 μ m, the maximum height was 5 μ m, and the minimum height was 1 μ m (Milner et al., 2012). The cell wall enclosed the cytoplasm and had a thickness of 6 nm (Wang et al., 2016). The maximum horizontal diameter of the nucleus was 5 μ m and the maximum height was 2 μ m (Table 2) (Figure 5) (Milner et al., 2012).

Table 2: Geometrical features of the osteoblast cell.

	Nucleus	Cytoplasm	Cell wall
Shape	Ellipse	Hat-form	Hat-form
Maximum diameter (µm)	5	20	N/A
Maximum height (µm)	2	5	N/A
Minimum height (µm)	N/A	1	N/A
Thickness (µm)	N/A	N/A	0.006

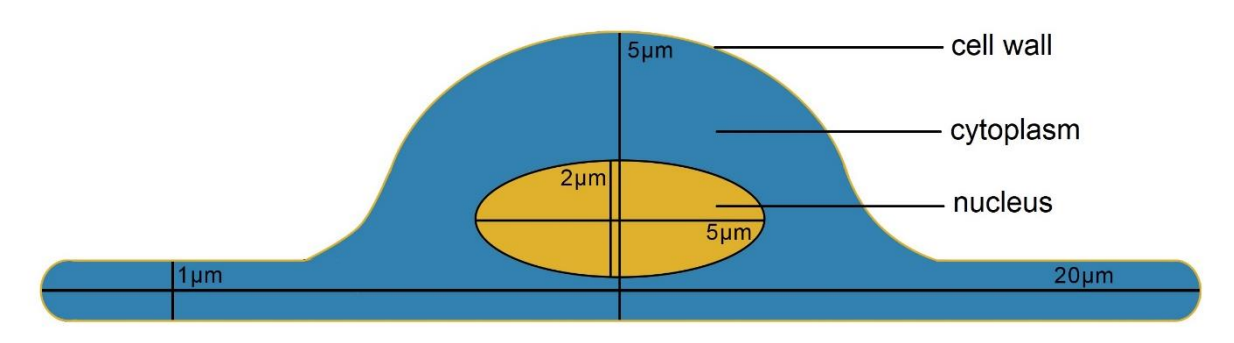


Figure 5: The geometric features of the osteoblast cell: the nucleus, the cytoplasm and the cell wall.

2.2.2 Material properties

The osteoblast cell was modelled consisting of a nucleus, cytoplasm and a cell wall. Both the nucleus and the cell wall of the osteoblast consisted of elastic properties (Wang et al., 2016). The cytoplasm of the osteoblast cell consisted of viscoelastic properties (Milner et al., 2012). FE models of the osteoblast cell were available in the literature (Milner et al., 2012; Wang et al., 2016). The elastic properties of the nucleus and the cell wall are listed in Table 6 (Wang et al., 2016). The nucleus had Young's modulus of 1.5 KPa and a Poisson's ratio of 0.37. The cell wall of the osteoblast had Young's modulus of 1 KPa and a Poisson's ratio of 0.3. In the study of Milner et al. (2012), the cytoplasm consisted of viscoelastic properties, like the cytoplasm of the bacterial cell. The material properties of the cytoplasm in our model of the osteoblast were the same as the viscoelastic properties for the cytoplasm of the bacterial cell, which were calculated in the previous section (Zhou et al., 2005).

Table 6: Coefficients of the material properties of the nucleus, cytoplasm and the cell wall of the osteoblast cell.

Nucleus of the osteoblast	Cytoplasm of the osteoblast		Cell wall of the osteoblast	
Elastic properties	Hyperelastic	Viscoelastic	Elastic properties	
	properties	properties		
	Neo-Hookean	Prony series		
	coefficients			
E = 1.5 KPa	$D10 = 6.21 * 10^5 MPa$	$g_1 = 0.39$	E = 1 KPa	
v = 0.37	D1 = 1666.7 MPa ⁻¹	$k_1 = 0$	v = 0.3	
		т = 18.75 s		

2.3 Nanopatterned surfaces

Different types of nanopatterned surface were tested. Nanopillars were the structures which were found on the wings of cicada and dragonfly (Diu et al., 2014; Ivanova et al., 2013).

2.3.1 Geometry

The geometry of the nanopatterned surface differed based on the height, interspace, width, radius and sharpness of the nanopillars (Figure 6). To evaluate the effect of each parameter, the most extreme values of each parameter found in the literature were implemented into the FE model (e.g., the smallest value found in the literature for width was 25 nm and the largest value for width was 200 nm) (Dickson et al., 2015; Dobbenga et al., 2016; Hasan et al., 2015; Wu et al., 2016). Furthermore, some intermediate values of the parameters were implemented. Table 3 gives an overview of the values of all the geometrical parameters.

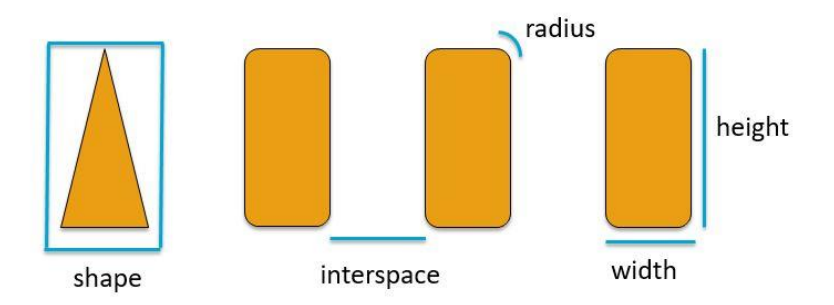


Figure 6: Geometrical parameters of the nanopatterned surface. The height (H), interspace (IS), width (W), radius (R) and shape are presented.

Table 3: Matrix with the values of the geometrical parameters of the nanopatterned surface.

Height (nm)	Interspace (nm)	Width (nm)	Radius (% of the width)	Shape
15	40	25	12.5%	Flattened
120	100	50	25%	Sharp
400	300	120	50%	
		200		

2.3.2 Material properties

The nanopatterned surface were fabricated using different types of materials. In the study of Jin et al. (2015) silicon nanopillars were fabricated with elastic properties. The Young's modulus of the nanopillars was 150 GPa and the Poisson's ratio was 0.278 (Table 7) (Jin et al., 2015). The difference between Young's modulus of the cell wall with respect to Young's modulus of the bacteria was large. The Young's modulus of the nanopillars was 25 million times bigger than Young's modulus of the bacterial wall. Three simulations of the interaction between the bacteria and the nanopatterned surface were performed with a reduced Young's modulus of the nanopillars. The decreased difference (ratio 250) between the Young's modulus of the bacterial wall and the nanopatterned surface showed an error percentage of 0.2% with the initial difference (ratio 25 million). These findings indicated that a decreased Young's modulus did not influence the results. This analysis can be found in the supplementary information (S2).

Table 7: Coefficients of the material properties of the nanopatterned surface.

Nanopillars
Elastic properties
E = 150 GPa
v = 0.278

2.4 Finite Element simulation

The FE model created in ABAQUS used a non-linear static/implicit analysis. This type of analysis could handle large deformations of the elements. A 2D model was used to create the interaction between Staphylococcus aureus or the osteoblast cell with the nanopatterned

surface. So far, no computational modelling of the interaction between a nanopatterned surface and cells had been found. Therefore, it was first necessary to create a simpler and fundamental model than to overcomplicate a model. Furthermore, the 2D model saved computational time. The 2D model needed an out-of-plane thickness for the geometries. For the simulation of Staphylococcus aureus with the nanopatterned surface, the out-of-plane thickness was 600 nm, the maximum diameter of Staphylococcus aureus. The out-of-plane thickness of 600 nm was applied on the nanopatterned surface and on Staphylococcus aureus. For the simulation of the osteoblast cell with the nanopatterned surface, the out-of-plane thickness was 20 μ m, the maximum diameter of the osteoblast cell. The out-of-plane thickness of 20 μ m was applied on the nanopatterned surface and the osteoblast cell.

2.4.1 Meshing

Meshing the model led to a subdivision of the model into elements. Every element had its equations which had to be solved. A high mesh resolution indicated that the model existed of many elements. The model would converge when the mesh resolution was increased (Panagiotopoulou et al., 2012). Convergence indicated the maximum number of elements was reached for the solution. More elements would result in the same solution. More elements resulted in more equations with a more considerable computational time. Mesh refinement was needed to determine the number of elements needed for a converged solution.

2.4.1.1 Interaction of the Staphylococcus aureus with the nanopatterned surface

The bacterial cell and the nanopatterned surface consisted both of quadratic quadrilateral elements (CPE8H and CPE8 elements). Furthermore, plain strain elements were used, which were often used in an analysis with non-linearity and hyperelasticity. Four different mesh sizes were tested: 1.95 nm, 3 nm, 4 nm and 5.25 nm. A smaller mesh size than 3 nm showed an error percentage less than 0.5% in comparison with the mesh size of 3 nm based on the average stress of a pillar. Indicating that the mesh size of 3 nm resulted in a converged solution of the FE simulation. Therefor the chosen mesh size for the model was 3 nm. The mesh refinement analysis can be found in the supplementary information (S4.1).

2.4.1.2 Interaction of the osteoblast with the nanopatterned surface

The osteoblast cell and the nanopatterned surface consisted of quadratic quadrilateral elements (CPE8 elements) and quadratic triangular elements (CPE6M elements). For this simulation, plain strain elements were used as well. Four different mesh sizes were tested: 6.5 nm, 10 nm, 12 nm and 14 nm. The error percentage of the mesh sizes smaller than 10 nm showed an error percentage less than 1% in comparison with the mesh size of 10 nm based on the average stress of a pillar. Indicating that the FE simulation was converged at a mesh size of 10 nm. Therefore, the chosen mesh size was 10 nm. The mesh refinement analysis can be found in the supplementary information (S4.2).

2.4.2 Loading, boundary conditions and interaction

During the experimental tests, the medium with dissolved Staphylococcus aureus or with dissolved osteoblast cells was displaced on top of the nanopatterned surface. The density of Staphylococcus aureus and the osteoblast cell was higher compared to the density of the medium. Due to the higher density, both cells would sink to the bottom. When both cells were in contact with the nanopatterned surface, they experienced the gravitational force of the mass of the cell itself and the gravitational force of the mass of the medium, which was above the

cell. This load was simulated in the model as a body force. The first body force was based on the gravitational force of the mass of the cell and the second body force was based on the gravitational force of the medium. The body force could be calculated by the following formula:

$$BF = \frac{m * g}{V} \tag{7}$$

Where m was the mass, g was the gravitational constant and V was the volume. Staphylococcus aureus was modelled into two parts: the cytoplasm and the cell wall. Therefore, the body force was divided into two body forces, each for a part. As already explained, the body forces were also based on the gravitational force of the mass of the bacteria and the mass of the belonging medium, so four body forces were applied for the simulation of the interaction of the nanopatterned surface with Staphylococcus aureus. The osteoblast cell was modelled into three parts: the nucleus, the cytoplasm and the cell wall. For the osteoblast cell, the body force was divided into three body forces. Also, the body force was based on the gravitational force of the mass of the osteoblast and the mass of the belonging medium, so six body forces were applied on the osteoblast cell for the simulation of the interaction of the nanopatterned surface with the osteoblast cell.

The body force applied on Staphylococcus aureus was divided between the cell wall and cytoplasm. Both the cell wall and the cytoplasm contained approximately 50% of the total mass of Staphylococcus aureus (Harris et al., 2002; Silhavy et al., 2010). The mass distributions influenced the body force and might influence the results of the simulation. Therefore, the mass distribution based on the body force had been examined. Three different mass distributions of the total mass of the bacterial cell were evaluated: 20% cytoplasm and 80% cell wall, 50% cytoplasm and 50% cell wall, and 80% cytoplasm and 20% cell wall. The difference between the three mass distributions was less than 1% based on the average stress of a pillar and was negligible. The mass distribution between the cell wall and the cytoplasm did not affect the outcome parameters of the simulation. However, the implemention of the cell wall resulted in a significant effect on the outcome parameters. The error percentage between the bacteria with a cell wall and cytoplasm was larger than 20% in comparision to the bacteria which was only made of cytoplasm. This large error percentage showed that the cell wall was an important feature, which should not be left out. The analysis can be found in the supplementory information (S4)

Boundary conditions were applied at the bottom of the nanopatterned surface. The nanopattern should not be able to move. Therefore the bottom was fixed. Some simulations had a nanopattern with a smaller height than the sinking depth of the bacteria or osteoblast. A platform was added to the bottom of the pillars, to prevent unreal situations (Figure 7). In reality, the surface of the implant resembled the platform. The platform was fixed as well.

Figure 7: Additional platform to the nanopillars, preventing the bacteria to sink further than the height of the pillars.

The interaction between the two different parts was specified (Staphylococcus aureus and the nanopatterned surface or the osteoblast and the nanopatterned surface) using contact property. For experimental tests the nanopatterned surface was created with techniques such as nanoimprint lithography or anodizing. These techniques resulted in a coarse surface area

of the nanopatterned surface. Therefor the type of contact property between the nanopatterned surface and both cells was modelled as tangential behaviour, with the friction formulation set as rough. The interaction between the nanopatterned surface and both cells allowed finite sliding and was based on a surface to surface discretization method. We assumed that the different parts of Staphylococcus aureus (cytoplasm and cell wall) and the different parts of the osteoblast cell (nucleus, cytoplasm and cell wall) were united. So no contact property was modelled between these individual parts.

2.4.2.1 Loading of Staphylococcus aureus

The mass of Staphylococcus aureus was one pg (Perry et al., 2002). The total volume of the bacterial cell was 0.0170 μm^3 . The volume of the cytoplasm was 0.159 μm^3 , and the volume of the bacterial wall was 0.011 μm^3 . It should be noted that the units in ABAQUS were based on a tonne for masses, millimeters for geometries and megapascal for stresses. The mass of the medium was in total 1.8 ng. In Table 8 the calculated body forces of Staphylococcus aureus are listed.

Table 8: Body forces of Staphylococcus aureus.

	Staphylococcus aureus		the medium	
Distribution of mass			BF _{cytoplasm}	BF _{wall} (N/mm ³)
			(N/mm³)	
100% cytoplasm	5.78 *10 ⁻⁵	N/A	0.104	N/A
20% cytoplasm, 80% cell wall	1.24 *10 ⁻⁵	7.06 *10 ⁻⁴	2.23 *10 ⁻²	1.270
50% cytoplasm, 50% cell wall	3.09 *10 ⁻⁵	4.41 *10 ⁻⁴	5.57 *10 ⁻²	0.794

1.76 *10-4

Body force based on the mass of Body force based on the mass of

8.91 *10-2

2.4.2.2 Osteoblast cell

4.95 *10-5

80% cytoplasm, 20% cell wall

The mass of the osteoblast cell was 1.48 ng (Milner et al., 2012; Wang et al., 2016). The osteoblast cell was modelled consisting of a nucleus, cytoplasm and a cell wall. All three parts had different densities (Wang et al., 2016). The masses of the different parts of the osteoblast cell were determined based on the volume and density of these parts (Table 9).

Table 9: Mass calculation of the nucleus, cytoplasm and cell wall of the osteoblast cell.

	Density (tonne/mm³)	Volume (mm³)	Mass (ng) m = ρ * V
Nucleus	1.8 *10 ⁻⁹	1.57 *10 ⁻⁷	0.283
Cytoplasm	1.5 *10 ⁻⁹	7.91 *10 ⁻⁷	1.19
Cell wall	0.6 *10 ⁻⁹	5.43 *10 ⁻⁹	3.26 *10 ⁻³

The calculations of the body force of the osteoblast cell are listed in Table 10. In contrast to the bacterial cell, no different distributions of the mass were evaluated. The distribution of the mass was already determined by the calculations of the mass of the nucleus, cytoplasm, and cell wall. Based on the ratio of the mass distribution of the osteoblast, the mass of the medium was distributed with the same ratio. Therefore the mass of the medium was multiplied by a factor representing the mass of a particular part in respect to the mass of the total osteoblast. The mass of the medium was multiplied by a factor of 0.192 $(\frac{0.283}{1.48})$ for the calculation of body

0.318

force applied to the nucleus. For the calculations of the body force of the cytoplasm, the mass of the medium was multiplied with a factor of 0.806 $(\frac{1.19}{1.48})$, and for the calcualtions of the cell wall of the osteoblast, the mass of the medium was multiplied with a factor of 0.002 $(\frac{0.0057}{1.48})$.

Table 10: Body forces of the osteoblast cell.

Body force based on the mass of the osteoblast

BF _{nucleus} (N)	BF _{cytoplasm} (N)	BF _{wall} (N)			
1.77 * 10 ⁻⁵	1.476 * 10 ⁻⁵	5.89 * 10 ⁻⁶			
Body force based on the mass of the medium					
BF _{nucleus}	BF _{cytoplasm}	BF _{wall}			
2.4 * 10 ⁻²	2 * 10 ⁻²	7.98 * 10 ⁻³			

2.4.3 Simulation setup

Twenty-six different simulations were performed for this study (Table 11). First, the interaction between Staphylococcus aureus with the nanopatterned surface was simulated. The parameters height, interspace, width, radius, and sharpness were variated. The height was examined by varying height while combining it with the extremes of the width (Table 12). The interspace was examined by varying the interspace, while taking the extremes of the width as well (Table 13). The width was tested by varying the width, while combining it with the extremes of the interspace (Table 14). The radius was tested by fixing all parameters and only varying the radius (Table 15). Lastly, the shape was examined for the nanopatterned surfaces with the extreme conditions for width and interspace (Table 16).

The best performing nanopatterned surfaces regarding the bactericidal properties were determined. The interaction between these nanopatterned surfaces and osteoblast cells was simulated as well. Based on the results of the interaction between Staphylococcus aureus and the nanopatterned surface, four nanopatterned surfaces were considered for testing the cytotoxicity of osteoblast cells (Table 17).

Table 11: Characteristics of the twenty-six simulations.

	Height (nm)	Interspace (nm)	Width (nm)	Radius (nm [% of the width])	Shape	Type of cell
Type 1	120	40	25	6.25 [25%]	Flattened	Staphylococcus aureus
Type 2	120	40	50	12.5 [25%]	Flattened	Staphylococcus aureus
Туре 3	120	40	120	30 [25%]	Flattened	Staphylococcus aureus
Type 4	120	40	200	60 [25%]	Flattened	Staphylococcus aureus
Type 5	120	300	25	6.25 [25%]	Flattened	Staphylococcus aureus
Type 6	120	300	50	12.5 [25%]	Flattened	Staphylococcus aureus
Type 7	120	300	120	30 [25%]	Flattened	Staphylococcus aureus
Type 8	120	300	200	60 [25%]	Flattened	Staphylococcus aureus
Туре 9	120	100	120	15 [12.5%]	Flattened	Staphylococcus aureus
Type 10	120	100	120	30 [25%]	Flattened	Staphylococcus aureus
Type 11	120	100	120	60 [50%]	Flattened	Staphylococcus aureus
Type 12	120	100	25	6.25 [25%]	Flattened	Staphylococcus aureus
Type 13	120	100	200	50 [25%]	Flattened	Staphylococcus aureus
Type 14	15	100	25	6.25 [25%]	Flattened	Staphylococcus aureus
Type 15	400	100	25	6.25 [25%]	Flattened	Staphylococcus aureus
Type 16	15	100	200	15	Flattened	Staphylococcus aureus
Type 17	400	100	200	50 [25%]	Flattened	Staphylococcus aureus
Type 18	120	40	120	N/A	Sharp	Staphylococcus aureus
Type 19	120	300	120	N/A	Sharp	Staphylococcus aureus
Type 20	120	100	50	12.5 [25%]	Flattened	Staphylococcus aureus
Type 21	120	100	200	N/A	Sharp	Staphylococcus aureus
Type 22	120	100	50	N/A	Sharp	Staphylococcus aureus
Type 23	120	300	25	6.25 [25%]	Flattened	Osteoblast cell
Type 24	120	300	50	12.5 [25%]	Flattened	Osteoblast cell
Type 25	120	300	120	30 [25%]	Flattened	Osteoblast cell
Type 26	15	100	25	6.25 [25%]	Flattened	Osteoblast cell

Table 12: Characteristics of the six simulations which examine the height of the nanopatterned surface.

Height (nm)	Interspace (nm)	Width (nm)	Radius (nm [% of the width])	Sharpness
15	100	25	6.25 [25%]	Flattened
120	100	25	6.25 [25%]	Flattened
400	100	25	6.25 [25%]	Flattened
15	100	200	50 [25%]	Flattened
120	100	200	50 [25%]	Flattened
400	100	200	50 [25%]	Flattened

Table 13: Characteristics of the six simulations which examine the interspace of the nanopatterned surface.

Interspace (nm)	Height (nm)	Width (nm)	Radius (nm [% of the width])	Sharpness
40	120	25	6.25 [25%]	Flattened
100	120	25	6.25 [25%]	Flattened
300	120	25	6.25 [25%]	Flattened
40	120	200	50 [25%]	Flattened
100	120	200	50 [25%]	Flattened
300	120	200	50 [25%]	Flattened

Table 14: Characteristics of the eight simulations which examine the width of the nanopatterned surface.

Width (nm)	Height (nm)	Interspace (nm)	Radius (nm [% of the width])	Sharpness
25	120	40	6.25 [25%]	Flattened
50	120	40	12.5 [25%]	Flattened
120	120	40	30 [25%]	Flattened
200	120	40	50 [25%]	Flattened
25	120	300	6.25 [25%]	Flattened
50	120	300	12.5 [25%]	Flattened
120	120	300	30 [25%]	Flattened
200	120	300	50 [25%]	Flattened

Table 15: Characteristics of the three simulations which examine the radius of the nanopatterned surface.

Radius (nm [% of the width]	6 Height (nm))	Interspace (nm)	Width (nm)	Sharpness
15 [12.5%]	120	100	120	Flattened
30 [25%]	120	100	120	Flattened
60 [50%]	120	100	120	Flattened

Table 16: Characteristics of the eight simulations which examine the sharpness of the nanopatterned surface.

Sharpness	Height (nm)	Interspace (nm)	Width (nm)	Radius (nm [% of the width])
Flattened	120	40	120	30 [25%]
Sharp	120	40	120	N/A
Flattened	120	300	120	30 [25%]
Sharp	120	300	120	N/A
Flattened	120	100	50	12.5 [25%]
Sharp	120	100	50	N/A
Flattened	120	100	200	50 [25%]
Sharp	120	100	200	N/A

Table 17: Characteristics of the nanopatterned surfaces which examine the cell-cytotoxicity of osteoblast cells.

Type of cell	Height (nm)	Interspace (nm)	Width (nm)	Radius (nm [% of the width])	Sharpness
Staphylococcus Aureus	120	300	25	6.25 [25%]	Flattened
Osteoblast	120	300	25	6.25 [25%]	Flattened
Staphylococcus Aureus	120	300	50	12.5 [25%]	Flattened
Osteoblast	120	300	50	12.5 [25%]	Flattened
Staphylococcus Aureus	120	300	120	30 [25%]	Flattened
Osteoblast	120	300	120	30 [25%]	Flattened
Staphylococcus Aureus	15	100	25	6.25 [25%]	Flattened
Osteoblast	15	100	25	6.25 [25%]	Flattened

2.5 Statistical analysis

The statistical analysis was performed with the program R (R Development Core Team), a language and environment for statistical computing. Statistical analysis was needed for the interpretation and evaluation of the data by using a mathematical model (Vincent, 2005). Different mathematical models were created to examine the interaction between the dimensional parameters and the outcome parameters. A linear regression model was used to test the correlation between the outcome parameters equivalent strain and sinking depth. An ANOVA (Analysis of Variance) test was performed to describe the correlations between the geometrical features and all their interactions with the equivalent strain, corresponding to the bactericidal effect. Lastly, a linear model in the logarithmic scale was created to test the relation between the interaction of geometrical features and the maximum equivalent strain. For all statistical models the significance level was set at p=0.05.

3. Results

Twenty-six simulations of the interaction of the nanopatterned surface with Staphylococcus aureus or the osteoblast cell were performed. The program Python was used to extract the data of interest from every simulation. The software MATLAB® was used for further data analysis. Four different variables were calculated: the average stress of a pillar, the sinking depth ratio of the bacteria, the maximum strain of the bacterial wall and the maximum stress of the bacterial wall. In the next sections, first the parametric study will be discussed. The five geometrical features (height, interspace, width, radius and shape) will be analysed based on the four outcome parameters. Then the rupture criterion for bacterial cells and host cells is discussed to determine the bactericidal and cytotoxic properties of the nanopatterned surface. Lastly, a statistical analysis is performed to show the significant relationship between geometrical features and the bactericidal effect.

3.1 Parametric study

Height, interspace, width, radius and shape were the five geometrical features of the nanopatterned surface. These geometrical features were evaluated based on four different outcome parameters. The first outcome parameter was the average stress of the nanopillar. The stresses of all the nodes of one pillar were extracted from the model. The one nanopillar was in all simulations the left nanopillar of the two nanopillars which were in first contact with the nanopatterned surface. The average of the stresses of the nodes belonging to the pillar was taken to determine the average stress of a pillar. The second outcome parameter was the sinking depth ratio. Calculation of the sinking depth ratio was performed by extracting the displacement of the lowest-middle point of the bacteria or osteoblast. The displacement was divided by the diameter of the bacteria or the osteoblast cell. Thirdly, the maximum equivalent strain in the bacterial wall was calculated as an outcome parameter. The components of the elastic strain were extracted of all the nodes of the bacterial wall to calculate the maximum strain in the bacterial wall. Based on the components of the elastic strain, the equivalent strain was calculated with the following formula (Kusters and Hendriks, 1994):

$$\varepsilon_{eq} = \frac{2}{3} \sqrt{\frac{3*(\varepsilon_{11}^2 + \varepsilon_{22}^2 + \varepsilon_{33}^2)}{2} + \frac{3*(\varepsilon_{12}^2)}{4}}$$
 (8)

The maximum of the equivalent strain resembled the maximum strain in the bacterial wall. The last outcome parameter was the maximum stress in the bacterial wall. The stresses of all the nodes in the bacterial wall were extracted. The maximum of these stresses resembled the maximum stress in the bacterial wall.

3.1.1 Height

Six different simulations were performed to examine the height. The height variated from 15, 120 to 400 nm. These three different heights were combined with the smallest width (25 nm) and the largest width (200 nm). All other dimensional parameters were kept constant and can be found in Table 12. Figure 8 shows the simulation with a nanopatterned surface with a height of 15 nm (a) and a height of 400 nm (b). The behaviour of the bacterial cell was almost similar for both nanopatterned surfaces. For the nanopatterned surface with a height of 15 nm, the bacterial cell fully adopted between the two pillars and even had contact with the flat surface of the substrate. This could be seen in the analysis as well, the sinking depth ratio of the nanopatterned surfaces with a height of 15 nm was lower in comparison with nanopatterned

surfaces with a height of 120 nm and 400 nm (Figure 9b). A larger height of the nanopillar resulted in a higher average stress in a pillar. However, this only applied when the width was small (25 nm). A large width did not result in a significant difference in the average stress of the pillar. Figure 9c illustrates that a smaller width resulted in a higher maximum strain for the bacterial wall. However, the variation of the height did not change the maximum strain in the bacterial wall. Only a small elevation of the maximum strain in the bacterial wall could be seen for the nanopatterned surface with a width of 25 nm and a height of 15 nm. A similar principle was applicable for the maximum stress in the bacterial wall. The stress in the bacterial wall was the highest for the nanopatterned surface with a height of 15 nm and a width of 25 nm.

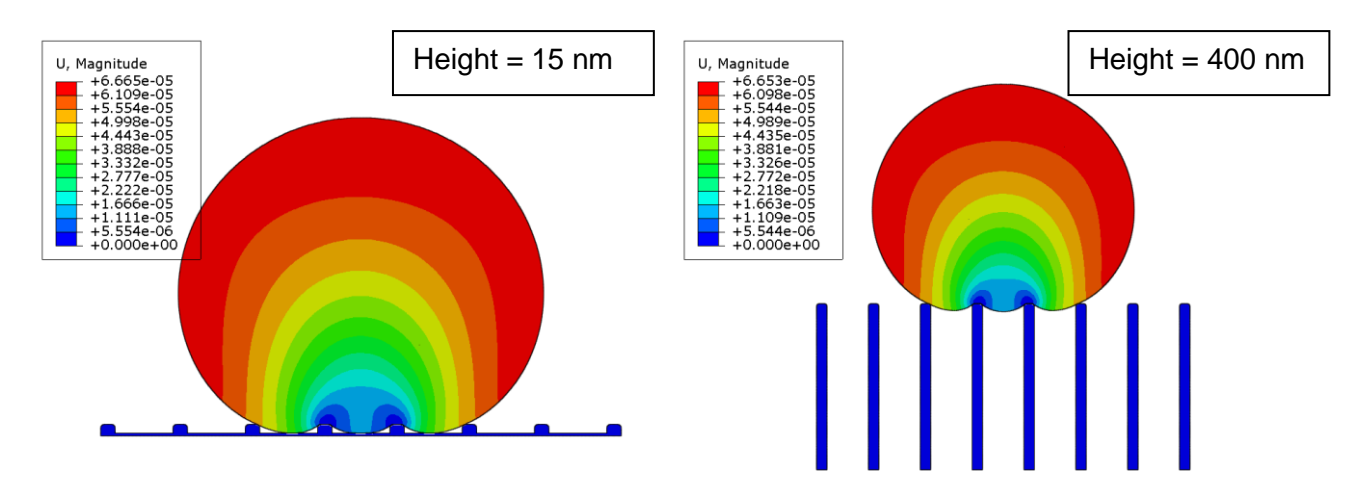


Figure 8: Distribution of magnitude of displacement in Staphylococcus aureus under similar loading conditions while the heights of the nanopillar changes. The simulations correspond to a) Type 14 b) Type 15 presented in Table 11.

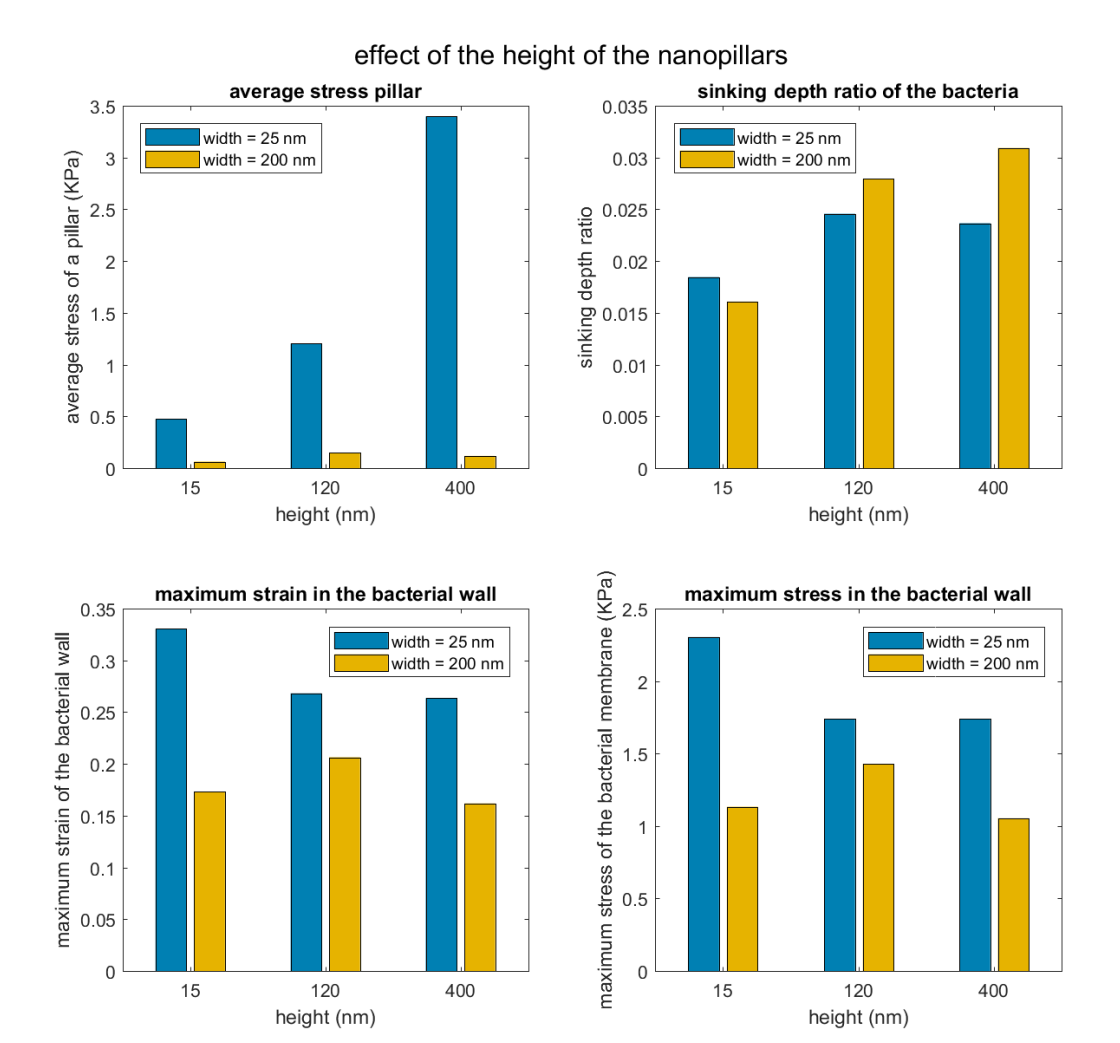


Figure 9: Analysis of the variable height of the nanopatterned surfaces. The x-axis represents the variation of height, while the blue bars show the variation of the nanopattern in combination with a small width (25 nm) and the orange bars show the variation of the nanopattern in combination with a large width (200 nm). a) average stress of a pillar. b) sinking depth ratio of the bacteria. c) maximum strain in the bacterial wall. d) maximum stress in the bacterial wall.

3.1.2 Interspace

Six different simulations were performed to examine the interspace. The interspace variated from 40, 100 to 300 nm. All three variations of the interspace were combined with the smallest width (25 nm) and the largest width (200 nm). Figure 10 shows the displacement of Staphylococcus aureus due to the nanopatterned surface with the smallest interspace and the nanopatterned surface with the largest interspace, both in combination with a width of 25 nm. The simulation of the nanopattern with an interspace of 40 nm showed that the bacterial cell responded to the nanopatterned surface like if it was in contact with a bed of nails. The bacteria found an equilibrium on top of the nanopattern. The nanopatterned surface with a large interspace showed the opposite (Figure 10b). The bacteria deformed between the pillars and at the outer sides of the nanopillars.

The larger the interspace, the higher the maximum strain and stress in the bacterial wall, particularly in combination with a small width. Also the sinking depth ratio and the average stress of a pillar was higher if the interspace was larger. The effect of the sinking depth ratio was almost similar for a width of 25 nm and a width of 200 nm. The effect of the average stress of a pillar, the effect of the maximum strain in the bacterial wall and the effect of the maximum

stress in the bacterial wall was stronger if the interspace was combined with a small width than when the interspace was combined with a large width (Figure 11).

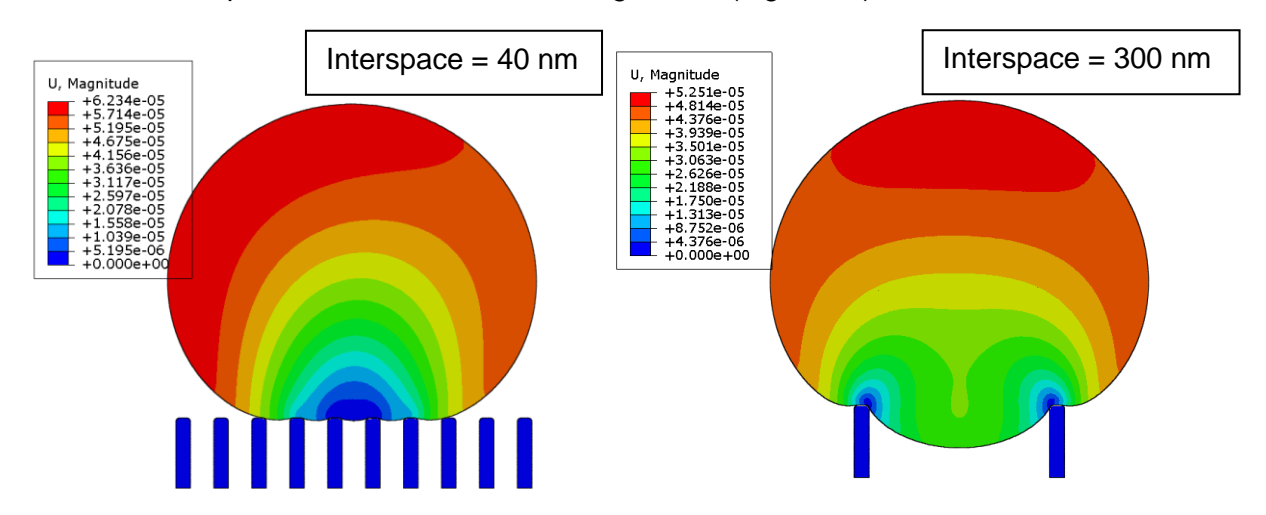


Figure 10: Distribution of magnitude of displacement in Staphylococcus aureus under similar loading conditions while the interspaces between the nanopillars changes. The simulations correspond to a) Type 1 b) Type 5 presented in Table 11.

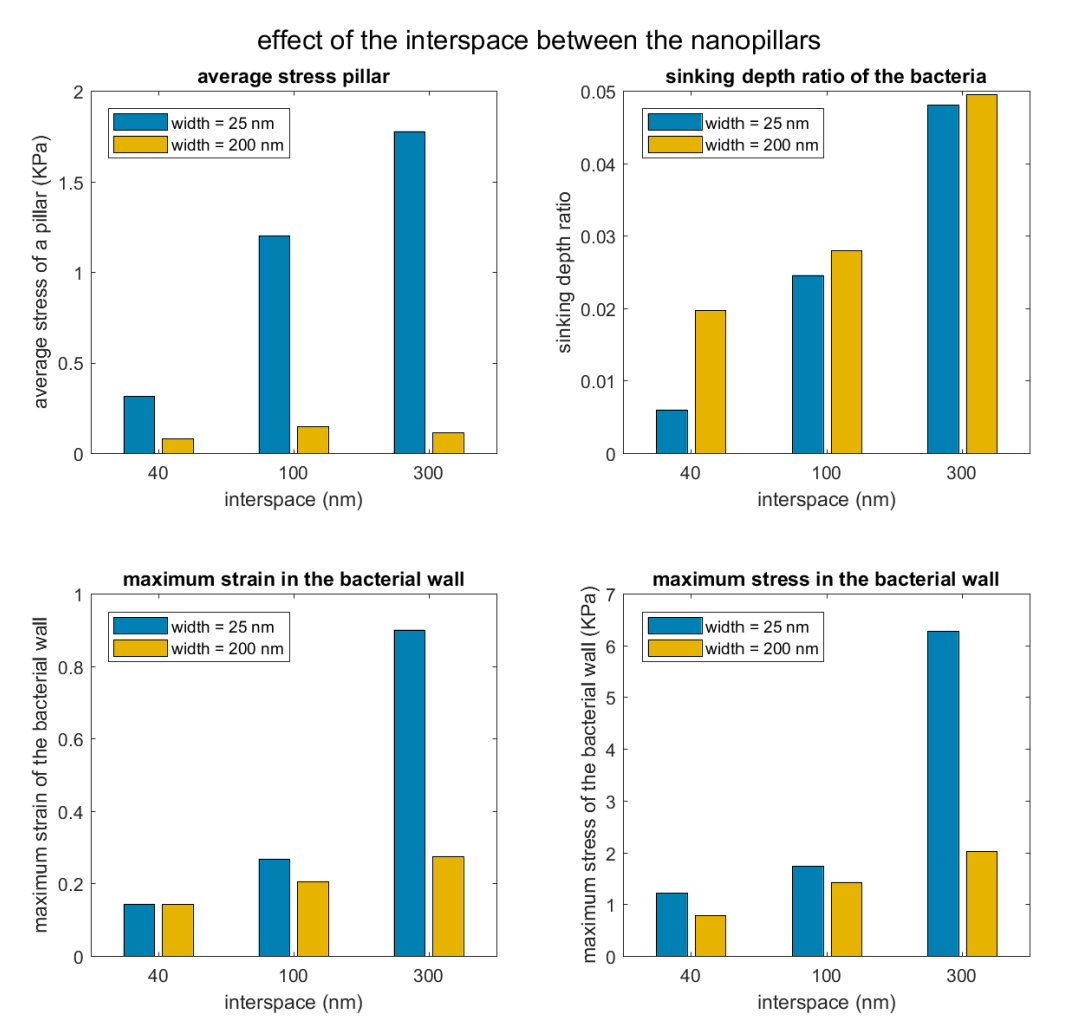


Figure 11: Analysis of the variable interspace of the nanopatterned surfaces. The x-axis represents the variation of interspace, while the blue bars show the variation of the nanopattern in combination with a small width (25 nm) and the orange bars show the variation of the nanopattern in combination with a large width (200 nm). a) average stress of a pillar. b) sinking depth ratio of the bacteria. c) maximum strain in the bacterial wall. d) maximum stress in the bacterial wall.

3.1.3 Width

Eight different simulations were performed to examine the width. The width variated from 25, 50, 120 to 200 nm. All four variations of width were combined with the smallest interspace (40 nm) and the largest interspace (300 nm). Figure 12 shows that the bacteria deformed between the pillars for a width of 25 nm and a width of 200 nm. For both simulations the sinking depth of the bacteria was about the same. However, during the simulation of the nanopillars with a width of 25 nm, the bacteria deformed at the outer sides of the nanopillars as well. When the interspace was small, the maximum strain and stress of the bacterial wall were almost similar (Figure 13). The average stress of the pillars increased when the width decreased. Due to the smaller area of the nanopillar, the stress could be distributed over fewer nodes. The sinking depth ratio increased when the width of the nanopatterned surface was larger, in combination with a small interspace. The larger the width, the lower the effect of the interspace on the behaviour of the bacterial cell. A smaller width resulted in higher strains and stresses in the bacterial wall, only in combination with a large interspace of the nanopillars. The width did not significantly influence the maximum stress and strain in the bacterial wall when the nanopattern was combined with a large interspace.

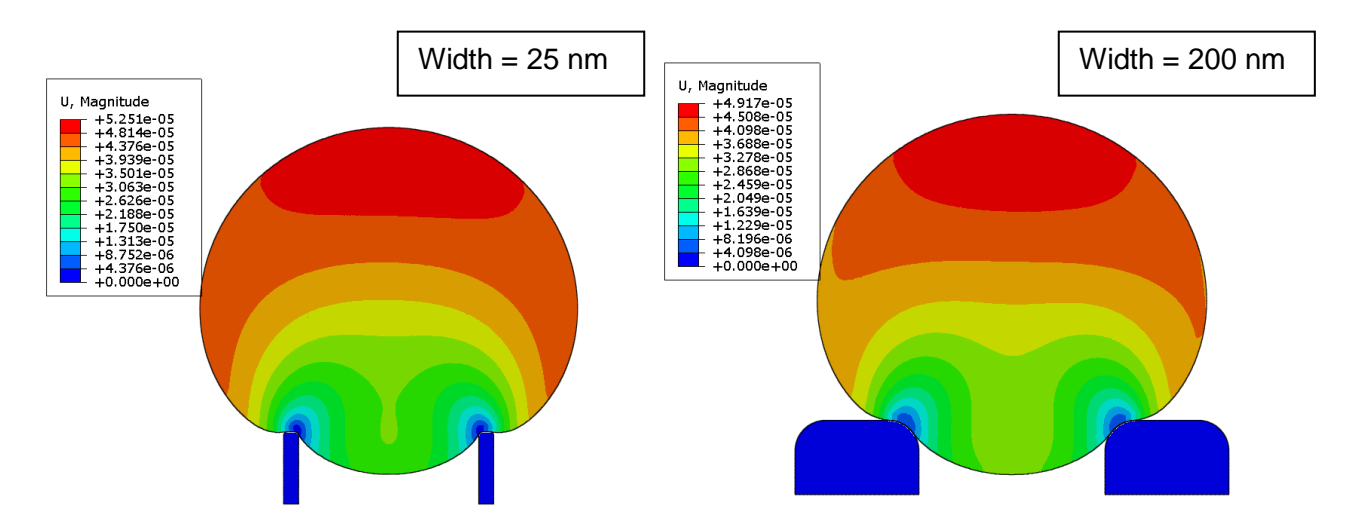


Figure 12: Distribution of magnitude of displacement in Staphylococcus aureus under similar loading conditions while the widths of the nanopillars changes. The simulations correspond to a) Type 5 b) Type 8 presented in Table 11.

effect of the width of the nanopillars average stress pillar sinking depth ratio of the bacteria 0.06 interspace = 40 nm interspace = 40 nm interspace = 300 nm interspace = 300 nm average stress of a pillar (KPa) 0.05 sinking depth ratio 0.04 0.03 0.02 0.5 0.01 0 0 25 50 120 200 25 120 200 width (nm) width (nm) maximum strain in the bacterial wall maximum stress in the bacterial wall maximum stress of the bacterial wall (KPa) maximum strain of the bacterial wall interspace = 40 nm interspace = 40 nm interspace = 300 nm 6 interspace = 300 nm 4 3 0.4 2 0.2 1

Figure 13: Analysis of the variable width of the nanopatterned surfaces. The x-axis represents the variation of width, while the blue bars show the variation of the nanopattern in combination with a small interspace (40 nm) and the orange bars show the variation of the nanopattern in combination with a large interspace (300 nm). a) average stress of a pillar. b) sinking depth ratio of the bacteria. c) maximum strain in the bacterial wall, d) maximum stress in the bacterial wall.

25

50

width (nm)

120

200

200

0

25

50

120

width (nm)

3.1.4 Radius

Three different simulations were performed to examine the radius of the pillars. The radius variated from 12.5%, 25% to 50% of the width. The percentage 50% indicated that the radius started at 50% of the width, showing a circular shape (Figure 14b). The percentage 25% indicated that the radius only occupied 25% of the width. For this nanopattern the flattened area occupied 50% of the total width. This also applied to the radius of 12.5%, although the flattened area occupied 75% of the total width (Figure 14a).

Figure 14 shows the difference between the nanopatterned surface with a radius of 12.5% of the width and a radius of 50% of the width for the nanopillars. The simulation with the nanopatterned surface with a radius of 50% showed a higher sinking depth than the simulation with a nanopatterned surface with a radius of 12.5%.

As can be seen from Figure 15, the effect of the radius on the outcome parameters was small. The smaller the radius of the nanopattern, the higher the average stress of a pillar and the higher the maximum strain and stress in the bacterial wall. The higher the radius of the nanopatterned surface, the higher the sinking depth ratio.

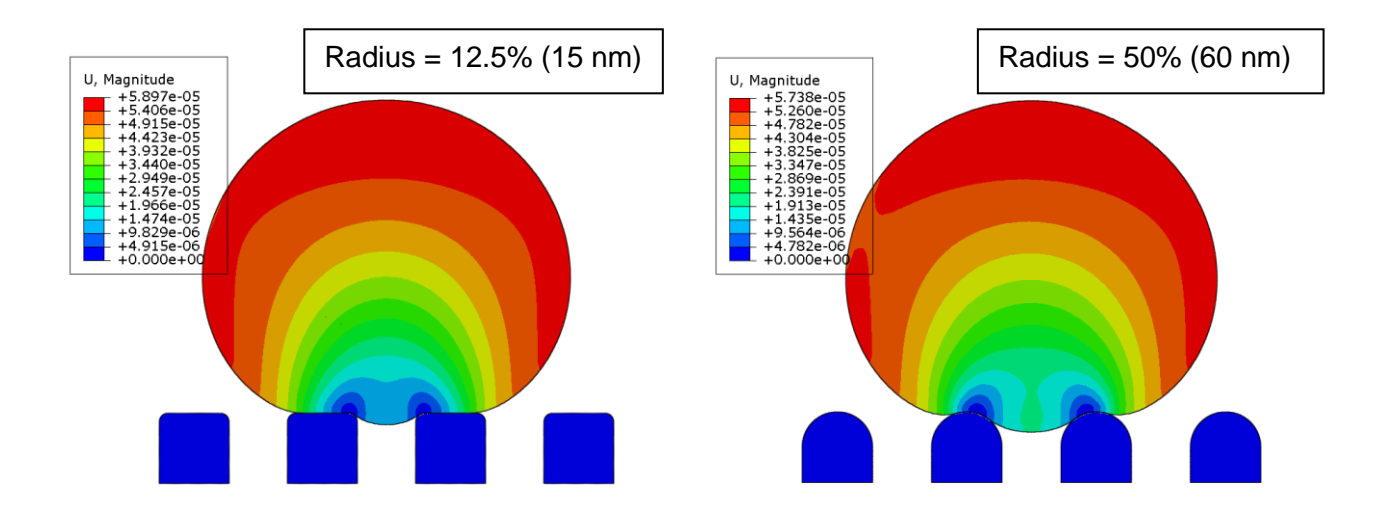


Figure 14: Distribution of magnitude of displacement in Staphylococcus aureus under similar loading conditions while the radii of the nanopillars changes. The simulations correspond to a) Type 9 b) Type 11 presented in Table

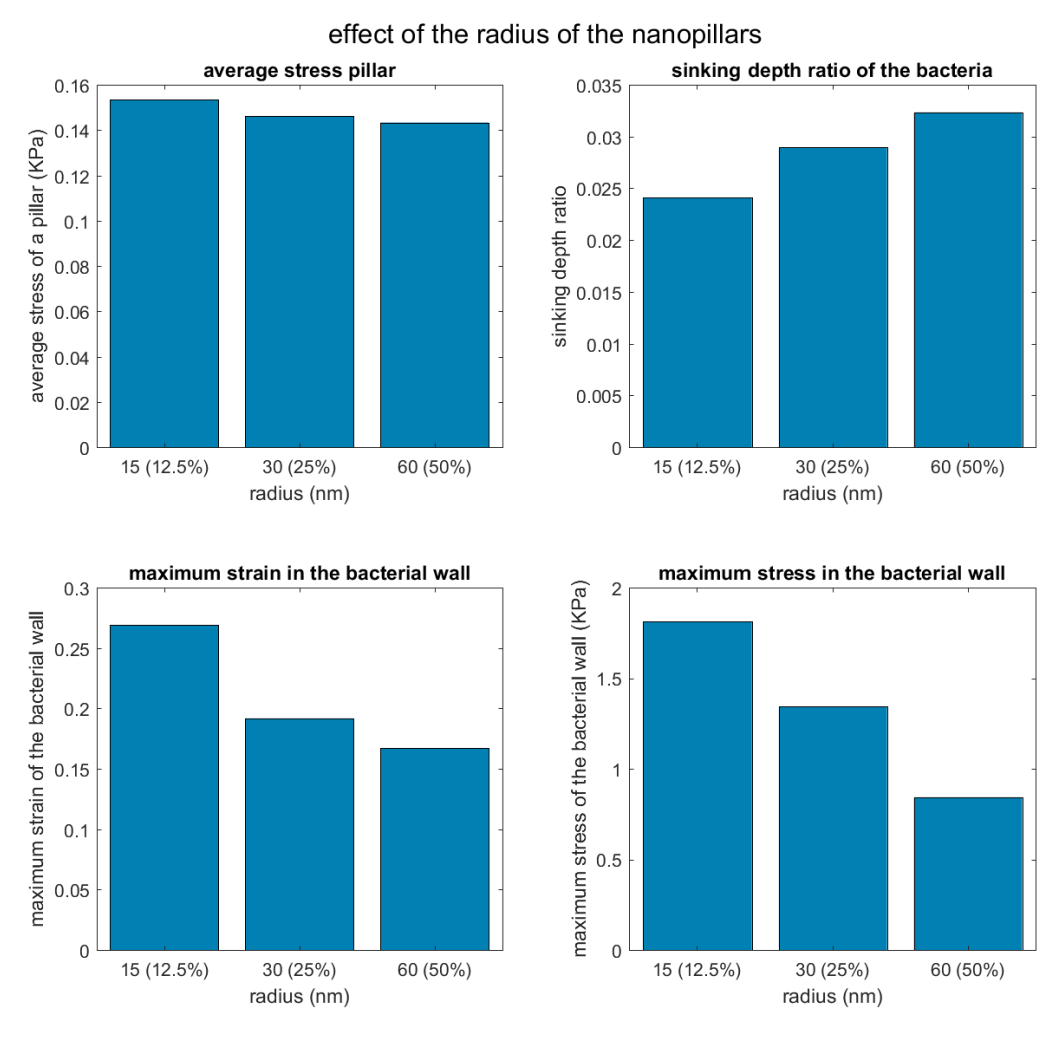


Figure 15: Analysis of the variable radius of the nanopatterned surfaces. The x-axis represents the variation of radius, while the blue bars show the variation of the nanopattern in combination with fixed parameters. a) average stress of a pillar. b) sinking depth ratio of the bacteria. c) maximum strain in the bacterial wall. d) maximum stress in the bacterial wall.

3.1.5 Shape

Eight different simulations were performed to examine the shape of the nanopatterned surface. Two different shapes were considered: a sharp nanopillar and a flat nanopillar (Figure 16). The flat nanopillar was used for previous simulations as well. The sharp and flattened nanopillars were tested for nanopatterned surfaces with the extremes of the width and interspace. So, the smallest and largest width were both combined with an intermediate interspace and the smallest and largest interspace were combined with an intermediate width resulting in four different nanopatterned surfaces.

The nanopatterned surface in Figure 16 had an interspace of 300 nm and a width of 120 nm. Figure 16 shows that the sinking depth was higher for the sharp nanopattern. This could be seen as well in Figure 17b, all sharp nanopillars showed a higher sinking depth ratio with respect to flattened nanopillars. The sharp nanopillared surfaces resulted two times in a higher maximum strain in the bacterial wall and one time in a higher maximum stress in the bacterial wall compared with the flattened nanopillared surfaces. The average stress in the pillars was three times higher for the sharp nanopillars in comparison with the flattened pillars. Due to the mixed results, the shape of the nanopatterned surface did not significantly influence the bactericidal properties of the nanopattern.

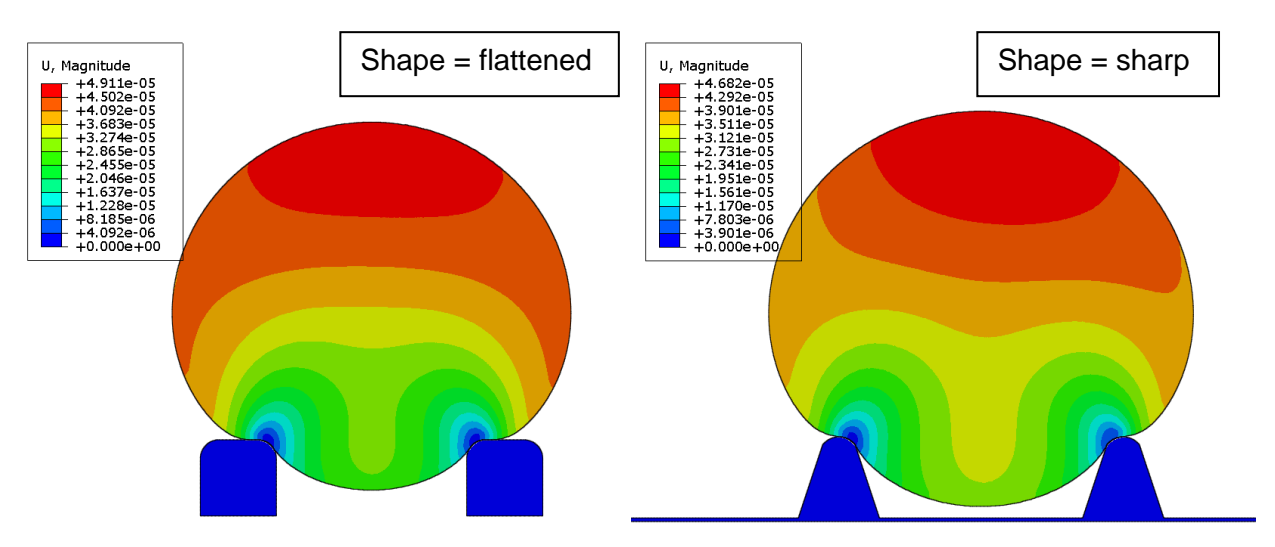


Figure 16: Distribution of magnitude of displacement in Staphylococcus aureus under similar loading conditions while the shapes of the nanopillars changes. The simulations correspond to a) Type 7 b) Type 19 presented in Table 11.

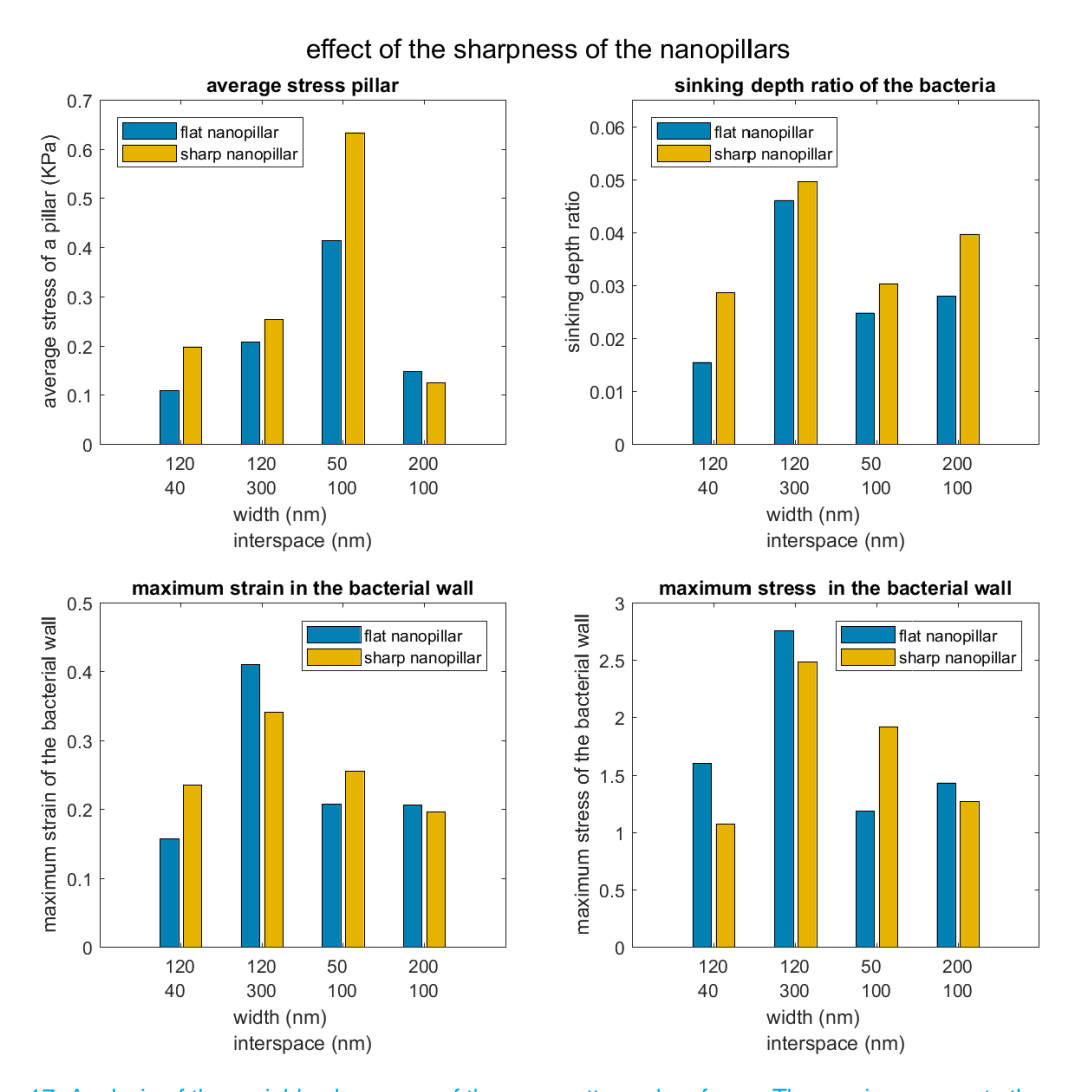


Figure 17: Analysis of the variable sharpness of the nanopatterned surfaces. The x-axis represents the variation in width and interspace, while the blue bars show the variation of the nanopattern in combination with a flattened nanopillar and the orange bars show the variation of the nanopattern in combination with a sharp nanopillar. a) average stress of a pillar. b) sinking depth ratio of the bacteria. c) maximum strain in the bacterial wall. d) maximum stress in the bacterial wall.

3.2 Von-mises strain criterion for the rupture detection of cells

In the previous section, the effect of nanopatterned surfaces on Staphylococcus aureus was examined, while changing geometrical features. In this section it is examined whether the simulated nanopatterned surfaces are bactericidal and/or cytotoxic. The nanopatterned surface was toxic for the cells if it broke the cell wall of Staphylococcus aureus. The cell wall of Staphylococcus aureus could break if the maximum strain in the cell wall exceeded its threshold. In that case the nanopatterned surface showed a bactericidal effect to Staphylococcus aureus. The same principle could be applied for osteoblast cells. The nanopatterned surface was cytotoxic if the cell wall of the osteoblast broke, by exceeding the strain threshold. In the literature it was found that the rupture strain of the cell wall of Staphylococcus aureus was 0.5 (Thwaites and Mendelson, 1985) and the rupture strain of the cell wall of the osteoblast cell was 1.05 (Li et al., 2013). In the next section the bactericidal effect and the cytotoxic effect of the nanopatterned surface are determined.

3.2.1 Bactericidal effects

Four nanopatterned surfaces with the highest maximum strain in the bacterial wall were considered for determination of its bactericidal effect. These four nanopatterned surfaces were indicated with type A - D. The specifics of these nanopatterns can be found in table 8.

Table 18: Characteristics of the nanopatterned surfaces which showed the highest bactericidal properties and are tested with the osteoblast cell.

	Height (nm)	Interspace (nm)	Width (nm)	Radius (nm [% of the width])	Shape
Type A	120	300	25	6.25 [25%]	Flattened
Туре В	120	300	50	12.5 [25%]	Flattened
Type C	120	300	120	30 [25%]	Flattened
Type D	15	100	25	6.25 [25%]	Flattened

In Figure 18 the maximum strain of the bacterial wall due to the four nanopatterned surfaces of type A-D (table 20) is shown. The threshold was set at a strain of 0.5, which would cause rupture of the bacterial wall (Thwaites and Mendelson, 1985). Nanopattern A and B exceeded the threshold for the rupture of the bacterial wall. Nanopattern C and D did not exceed the rupture threshold. The nanopatterned surface of type A and B could be seen as bactericidal, because they were able to rupture the bacterial wall.

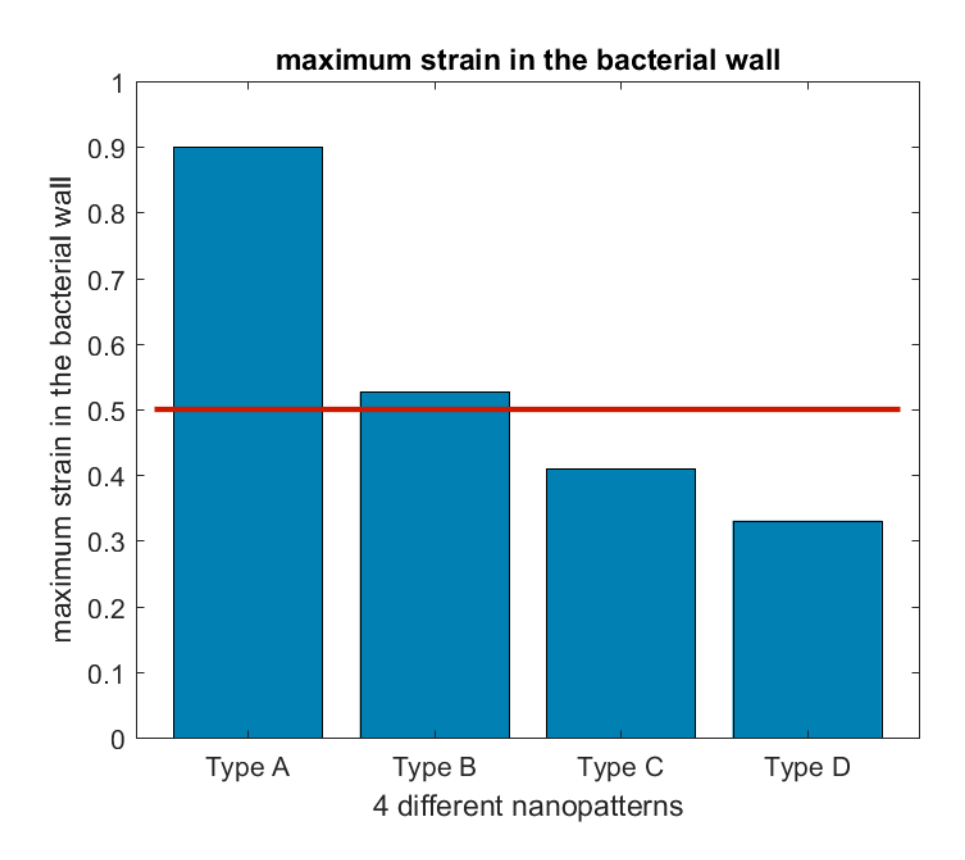


Figure 18: Threshold criteria for the rupture of the cell wall of Staphylococcus aureus based on the maximum strain in the cell wall.

3.2.2 Cytotoxic determination of host cells

Four simulations were performed to examine the cell cytotoxicity of osteoblast cells. These four simulation were determined based on the nanopatterned surfaces which showed the highest maximum strain in the bacterial wall. Table 18 shows these four different nanopatterns which were indicated by type A-D.

Figure 19 represents the deformed osteoblast cell on a nanopatterned surface. Due to the large scale of the osteoblast cell, it was difficult to see the deformation at the nanopatterned surface. Therefore, Figure 19b represents the interaction between the nanopillars and the osteoblast cell zoomed in. In Figure 20, the comparison between the osteoblast cell and Staphylococcus aureus is illustrated. The maximum strain in the cell wall of the osteoblast cells was higher for all four nanopatterns. While the maximum stress in the cell wall of the osteoblast cell was significantly less. Also the sinking depth ratio of the osteoblast cells was less. The lower sinking depth ratio of the osteoblast cells was due to the normalisation which was based on the diameter of the cell. The average stress of a pillar was higher for the osteoblast cell if the width of the nanopillars was larger than 50 nm. If the width was 25 nm, then the average stress of the pillar was higher for the simulation with the bacterial cell.

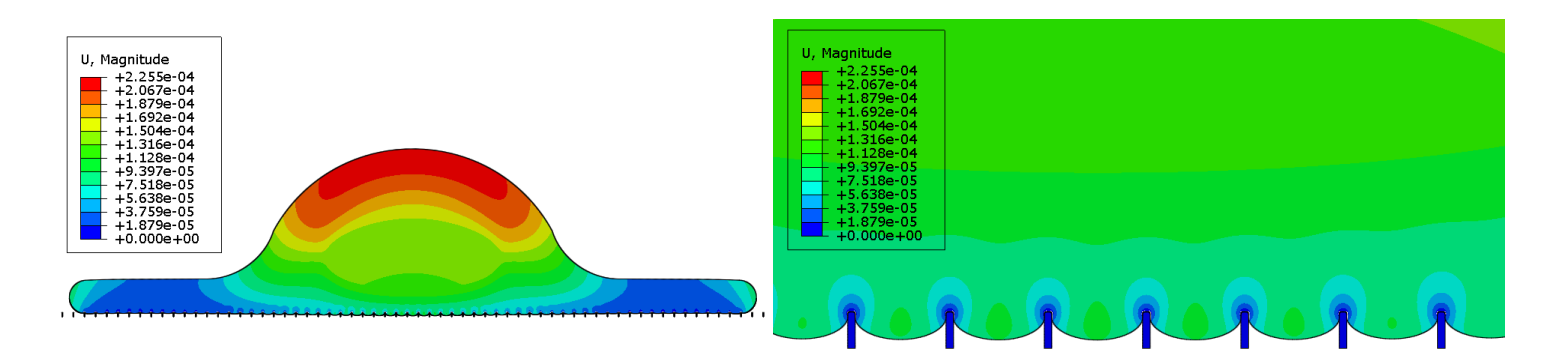


Figure 19: Distribution of magnitude of displacement in the osteoblast cell. a) Type 23 b) Zoomed in version of type 23 presented in Table 11.

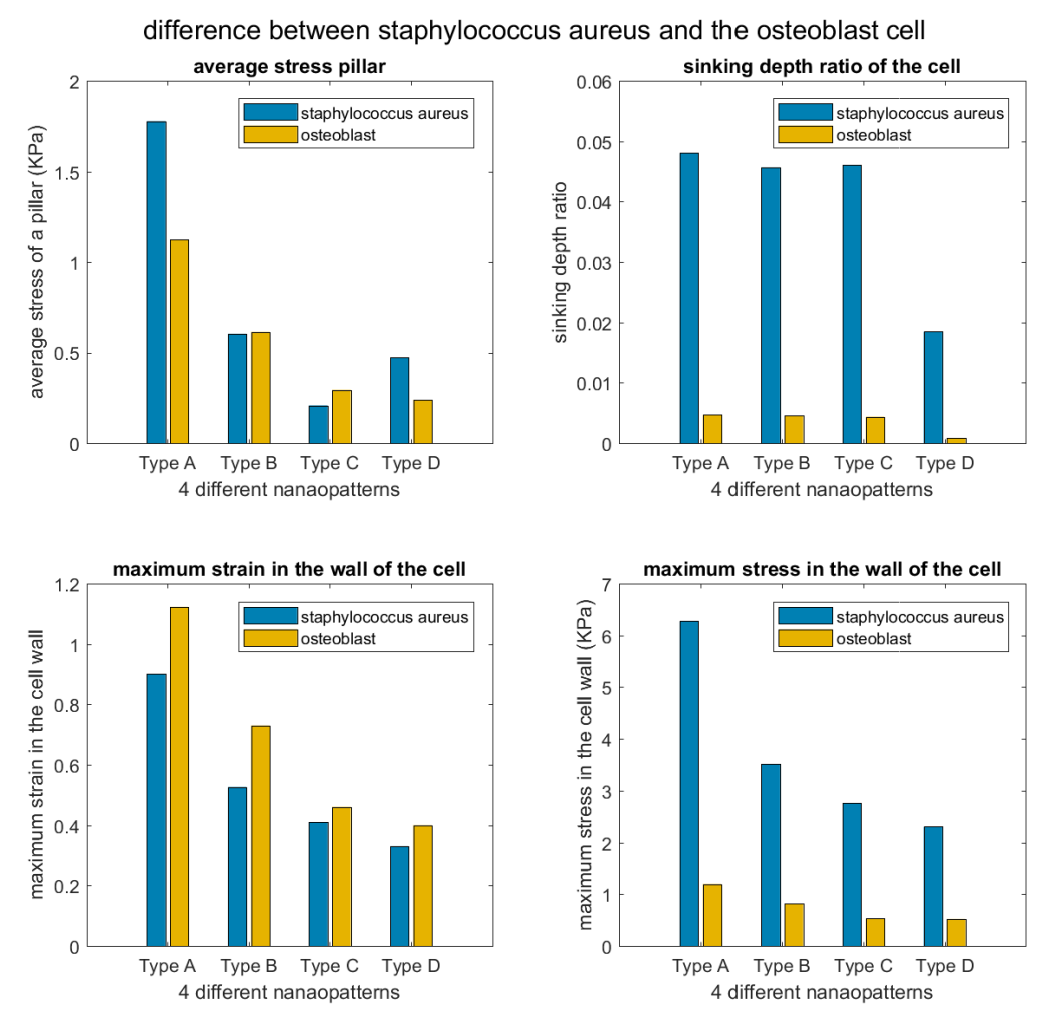


Figure 20: Analysis between the behaviour of the osteoblast and Staphylococcus aureus in response to 4 different nanopatterned surfaces presented in table 18. The x-axis represents the variation of different nanopatterns, while the blue bars show the response of Staphylococcus aureus and the orange bars show the response of the osteoblast cell. a) average stress of a pillar b) sinking depth ratio of the bacteria c) maximum strain in the bacterial wall.

The cytotoxic effect of these nanopatterned surfaces were examined based on the maximum strain in the cell wall of the osteoblast cell. Figure 21 shows the maximum strain in the cell wall of the osteoblast cell of the four different nanopatterned surfaces. The threshold for the rupture of osteoblast cells was set at 1.05 (Li et al., 2013). Type A was the only nanopatterned surface which exceeded the threshold. Nanopattern type A was cytotoxic for osteoblast cells. The nanopatterned surface of type B, C and D did not exceed the rupturing threshold. The nanopattern of type B, C and D were non-cytotoxic for osteoblast cells.

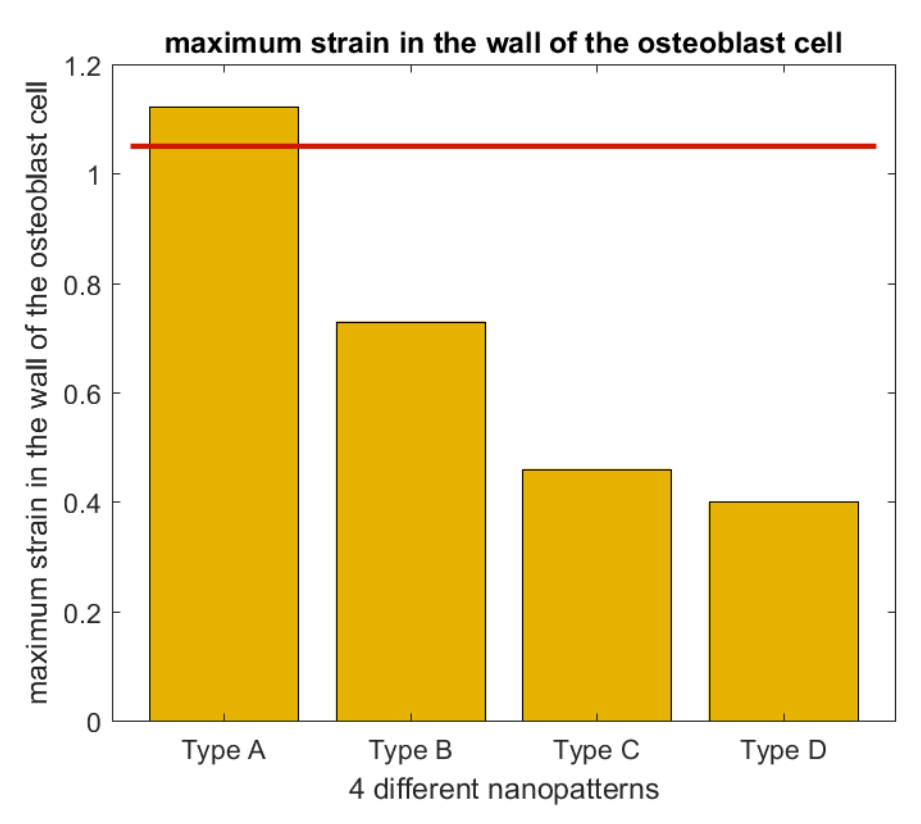


Figure 21: Threshold criteria for the rupture of the cell wall of osteoblast cells based on the maximum strain in the cell wall.

Figure 22 represents the normalized strain thresholds of both Staphylococcus aureus and the osteoblast cell. This figure shows that a nanopatterned surface of type A (a small width and a large interspace) resulted in bactericidal properties, but also in cytotoxic properties against the osteoblast cell. Type B (small/intermediate width and a large interspace) showed bactericidal properties against Staphylococcus aureus as well, but did not show cytotoxic properties against the osteoblast cell. Type C (intermediate/large width and a large interspace) and type D (small height and intermediate interspace) both did not show cytotoxic properties against Staphylococcus aureus and osteoblast cells.

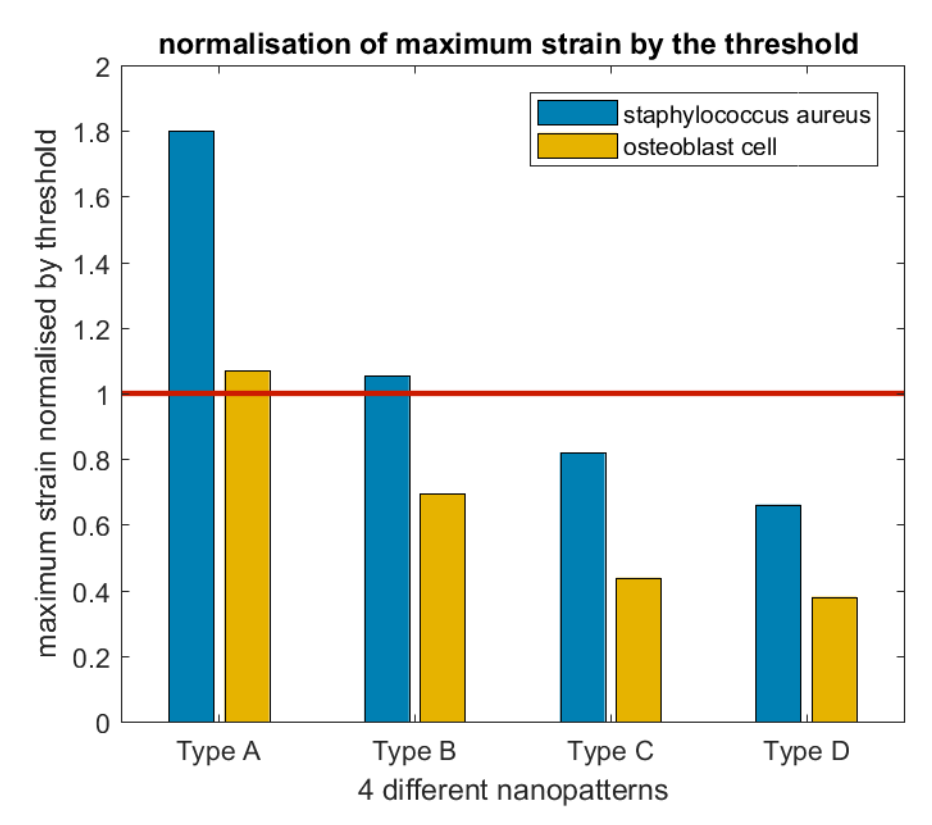


Figure 22: Normalized strain criteria for the rupture of the cell wall of Staphylococcus aureus and the osteoblast cell. The x-axis shows the different types of nanopatterned surfaces presented in table 18. The blue bars represent the maximum strain in the cell wall of Staphylococcus aureus normalized by its threshold and the orange bars represents the maximum strain in the cell wall of the osteoblast, normalized by its threshold.

3.3 Statistical models

The results of the geometrical features were already shown in the previous sections. The statistical tests in the next sections were performed to show the significance of the analysis. The first statistical model described the relation between the sinking depth of the bacteria and the maximum strain in the bacterial wall using a linear regression model. The second statistical test was an ANOVA (Analysis Of Variance) test, describing the correlations between the geometrical features and all their interactions with the maximum strain in the bacterial wall. For the third and fourth statistical tests a linear model in a logarithmic scale was used to describe the relations of the ratio of width and interspace and the ratio of radius and interspace with the maximum strain in the bacterial wall. The geometrical feature sharpness was not statistically tested because sharpness was a categorical variable, while the other variables were all quantitative variables.

3.3.1 Correlation between maximum strain and sinking depth

The first statistical model described the relations between the sinking depth and the maximum strain in the bacterial wall. The relationship between these two parameters was described using a linear regression model as:

$$Maximum\ strain = coef * SD \tag{9}$$

With a coefficient of 0.01351, an R² (goodness of fit) of 34.3% and a p-value (significance level) of 0.002 (Figure 23). Since maximum strain was correlated to the maximum applied force and material model, the sinking depth was also correlated and limited to those properties that we

assumed in the simulations (section 2). In this research, the maximum strain was taken as a criterion for the rupture of bacterial cells. Due to the linear relationship we find here between strain and sinking depth, an equivalent criterion based on sinking depth could be used for the prediction of the failure of bacterial cells. This is important as measuring sinking depth is more practical in the experimental procedures.

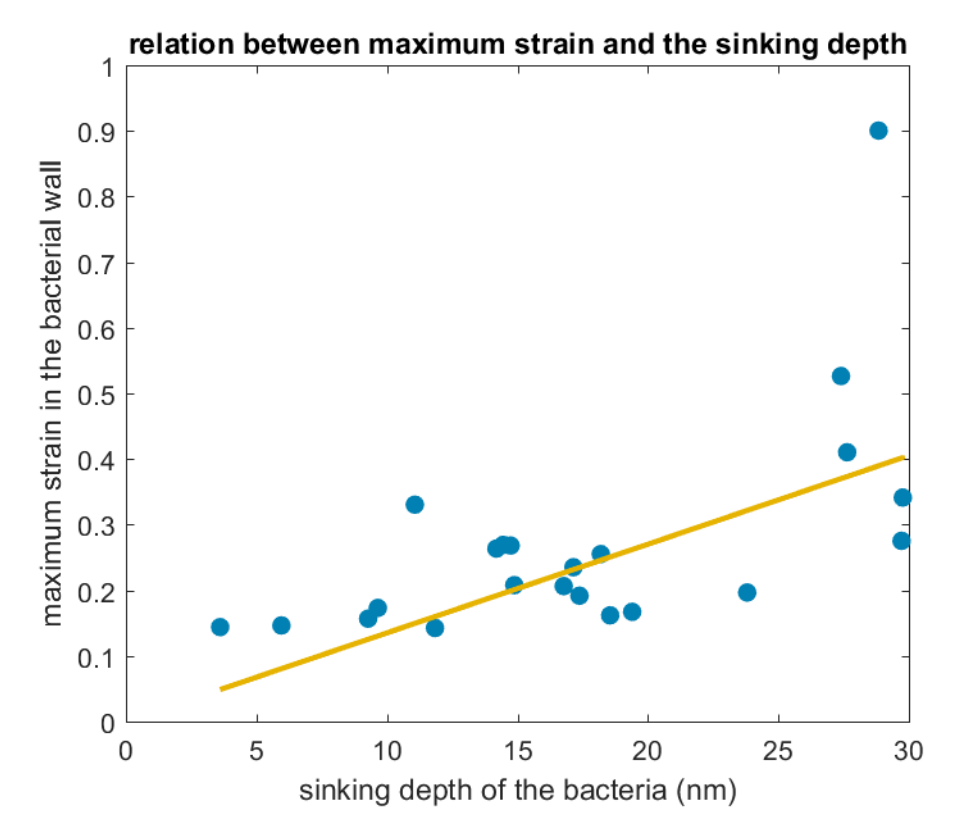


Figure 23: Statistical model of the relation between the sinking depth of the bacteria and the maximum strain in the bacterial wall. The x-axis shows the sinking depth ratio of the bacteria in nanometers, while the y-axis shows the maximum strain in the bacterial wall.

3.3.2 ANOVA-test

The second statistical test was an ANOVA test. This test took into account the effect of the variables height, interspace, width and radius. Height did not significantly influence the maximum strain in the bacterial wall. Radius, interspace, width and all their interactions between radius, width and interspace did affect the maximum strain in the bacterial wall. Table 19 shows the coefficients of the interactions of the geometrical features. The ANOVA test had an R (goodness of fit) of 96.65% and a p-value (level of significance) <0.0001.

Table 19: Coefficients of the ANOVA fitting the linear model

Coefficients of the ANOVA						
R	1.238625e-01					
IS	5.421990e-03					
W	-2.117803e-02					
R:IS	-1.270479e-03					
R:W	-2.370542e-04					
IS:W	2.053479e-04					
R:IS:W	2.518940e-06					

The ANOVA test showed the significant effect of the geometrical features of the radius, interspace and the width on the maximum strain. Also the interactions between radius, interspace and width showed significant effects on the maximum strain. Therefore, in the next two subsections, the ratio of width and interspace and the ratio of radius and interspace are statistically tested.

3.3.3 Correlation between the maximum strain and the ratio of width and interspace

The effect of the ratio between the width (W) and interspace (IS) on the maximum strain in the bacterial wall was examined using a linear model in a logarithmic scale. The ratio of these geometrical features was $\frac{W}{W+IS}$, describing a ratio between the surface area where the bacteria adhered on and the surface area where the bacteria could not adhere on. The model described the relation between the ratio $\frac{W}{W+IS}$ and the maximum strain in the bacterial wall, using the following formula:

$$Maximum strain = A_0 * (\frac{W}{W + IS})^{a_1}$$
 (10)

Where A_0 was $e^{\cdot 2.00854}$ and a_1 was -0.62077. The R^2 (goodness of fit) was 70.76% and the p-value (significance level) < 0.0001. The ratio $\frac{W}{W+IS}$ had a significant effect on the maximum strain in the bacterial wall (Figure 24). The lower the ratio $\frac{W}{W+IS}$, the higher the maximum strain in the bacterial wall. So if the width was fixed, a larger interspace would lead to a higher maximum strain and a smaller interspace would lead to a lower maximum strain. The interspace could be fixed as well, a small width would result in a higher maximum strain and a large width would result in a low maximum strain.

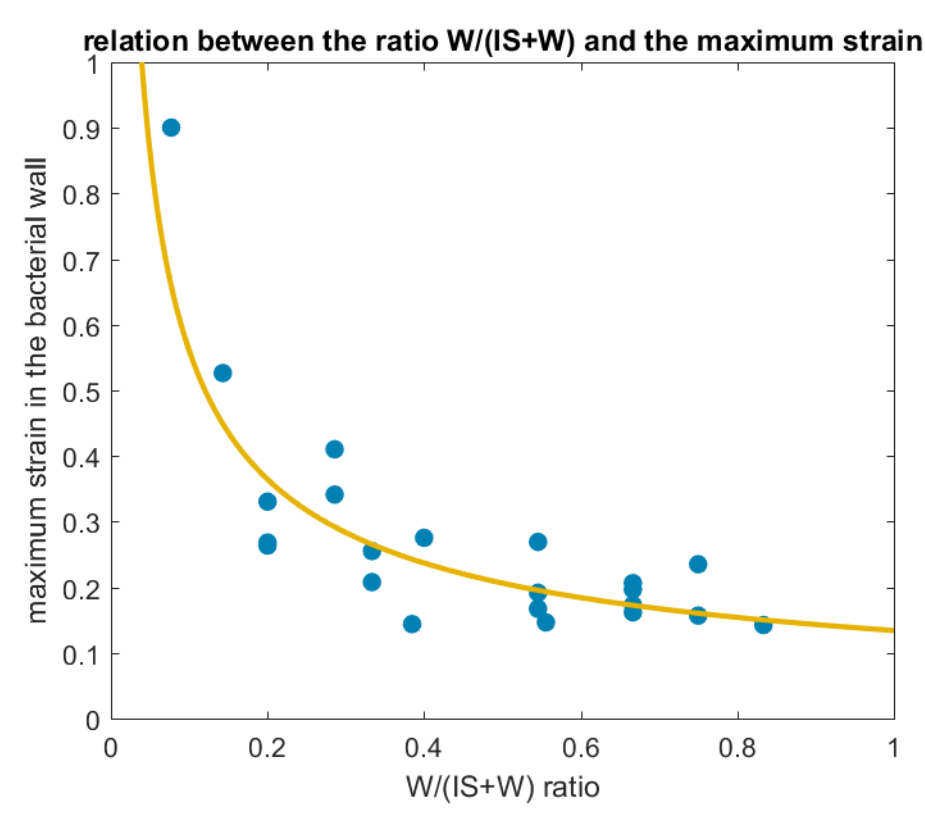


Figure 24: Statistical model of the relation between the ratio $\frac{W}{W+IS}$ and the maximum strain in the bacterial wall. The x-axis shows a ratio between the width and the interspace of the nanopattern, while the y-axis shows the maximum strain in the bacterial wall.

3.3.4 Correlation between the maximum strain and the ratio of radius and interspace

Besides the ratio between width and interspace, the effect of the ratio between radius (R) and interspace (IS) on the maximum strain in the bacterial wall was examined as well. The ratio $\frac{R}{IS}$ was tested using a linear model with a logarithmic scale. The model described the relation between the ratio $\frac{R}{IS}$ and the maximum strain in the bacterial wall with the following formula:

$$Maximum \ strain = B_0 * (\frac{R}{IS})^{b_1}$$
 (11)

Where B_0 was -2.07 and b_1 was -0.36. The R^2 (goodness of fit) was 64.7% and the p-value (significance level) < 0.0001. The ratio $\frac{R}{IS}$ had a significant effect on the bacterial wall (Figure 25). The lower the ratio $\frac{R}{IS}$, the higher the maximum strain in the bacterial wall. So, if the interspace was fixed, the variations of radius would lead to a high maximum strain if the radius was small and a low maximum strain if the radius was large. The radius could be fixed as well, then a small interspace resulted in a low maximum strain, and a large interspace resulted in a high maximum strain.

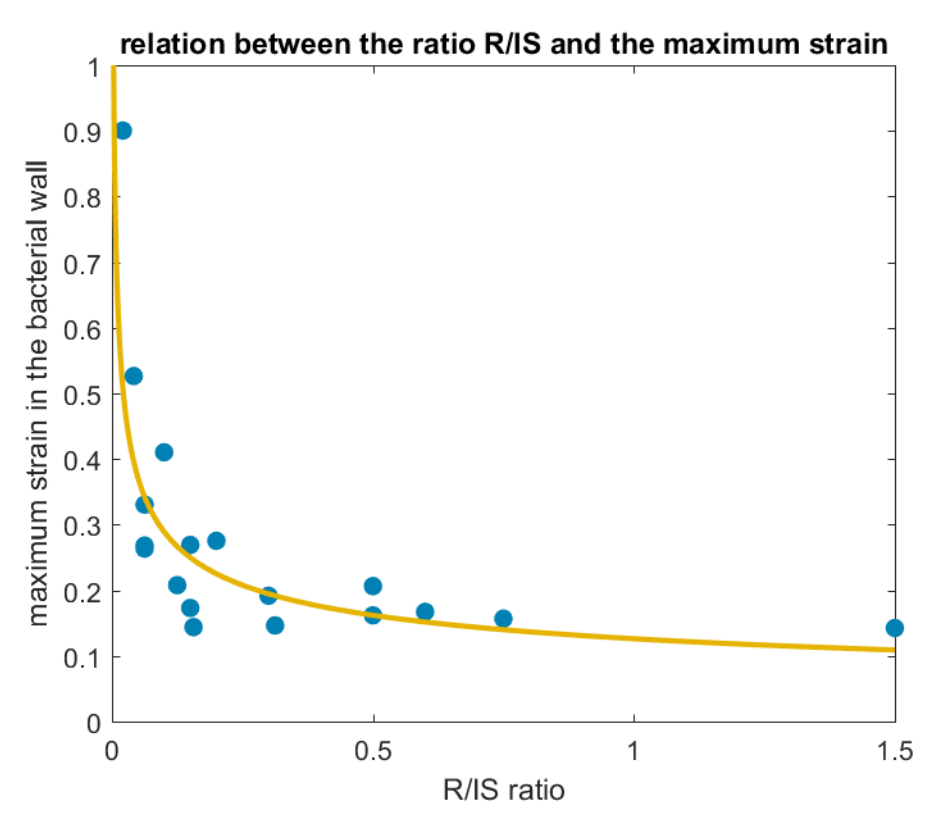


Figure 25: Statistical model of the relation between the ratio $\frac{R}{IS}$ and the maximum strain in the bacterial wall. The x-axis shows the ratio between radius and interspace of the nanopatterned surface, while the y-axis shows the maximum strain in the bacterial wall.

4. Discussion

Simulations of the interaction of nanopatterned surfaces with Staphylococcus aureus and the osteoblast cell were performed with different geometrical features for the nanopattern. The effect of the variables height, interspace, width, radius and the shape of the nanopattern have been examined. Firstly, the effect of the geometrical features of the nanopatterned surface on the host cells and bacteria's fate is discussed. Then the difficulties and validation of the FE model will be addressed. Lastly, some recommendations for future research will be given.

4.1 Effects of geometrical features of nanopatterned surface on the host cells and bacteria's fate

Five geometrical features were examined in this study: height, interspace, width, radius and shape. Also intervariability between the geometrical features was examined. Table 20 represents an overview of the geometrical features and their effect on the bactericidal properties of the nanopatterned surface. The parameter height did not significantly affect the bactericidal properties. The change in radius showed a small but significant effect on the outcome parameters as well. When the radius of the nanopatterned surface was decreased, the nanopatterned surface showed a small increase in bactericidal properties.

It was more difficult to determine the bactericidal effect of the shape. The sharp nanopatterned surfaces had to be circular at the top of the nanopillar. Otherwise computational errors occurred during the simulation. By making triangles with a round top, those computational errors could be prevented. Although the effect of the sharp nanopillar would be slightly faded, because the nanopillar would be more flattened due to the circular top. Two of the four nanopatterns showed a higher bactericidal activity due to the sharp nanopillared surfaces. These effects were found for the nanopatterned surfaces with a small width and a small interspace. This effect might be based on the deformation of the bacteria between the two nanopillars, while the bacteria also deformed at the outer parts of the nanopillars. This is in contradiction with the nanopillars with a large width and a large interspace. The bacteria would not deform at the outer parts of the nanopillars, because the bacteria was too small with respect to the large width of these nanopillars. Furthermore, the effect was probably stronger if the sharpness of the nanopillars was increased. A sharper nanopillar had a smaller effective surface area where the bacteria could adhere on (Hizal et al., 2015). Therefore, the bacteria had to deform directly after contact. Also, the deformation at the outer parts of the nanopillar could occur if the nanopillar was sharper and still had a large width. This would lead to a higher stretching degree and higher bactericidal properties of the nanopatterned surface. The effect of the shape of the nanopillar on the bactericidal properties showed some contrary results. Also the shape could not be implemented into the statistical models, therefore the effect of the shape remained unknown. Xue et al. (2015) and Tripathy et al. (2017) stated that a higher sharpness of the nanostructures resulted in higher bactericidal properties. Our results confirmed this statement only if the interspace and the width of the nanopillars were low. Additional analytical research should be performed to confirm the effect of shape of the nanopatterned surface on the bactericidal properties.

Table 20: Overview of the influence of the geometrical features obtained by the finite element model compared with the statements made in the literature.

Variable	Statements based of	Statements mad	Statements made by the literature			
Height	The height did not signifluence the bacterio		A larger height of the nanopillars resulted in higher bactericidal properties (X. Li, 2016)			
Interspace	influenced the bacter The larger the intersp nanopillars, the higher	interspace significantly enced the bactericidal properties. larger the interspace of the opillars, the higher the bactericidal perties. If the interspace was		A reduced interspace between the nanostructures resulted in a higher bactericidal effect (Kelleher et al., 2015) Nanopatterned surfaces with a higher nanopillar density showed higher bactericidal properties (Li, 2016)		
	combined with a small width, this effect was much stronger than when the interspace was combined with a large width		A larger interspace enhanced the back A large spacing be	A larger interspace between the nanostructures enhanced the bactericidal properties (Xue et al., 2015) A large spacing between the nanofeatures enhanced the bactericidal efficacy (Tripathy et al., 2017)		
Width	The width significantly bactericidal properties the width of the nano higher the bactericidate only in combination winterspace.	Nanopatterned 30	Nanopatterned surfaces with a higher nanopillar density showed higher bactericidal properties (Tripathy et al., 2017)			
Radius	The radius significant bactericidal propertie radius of the nanopill small increase of the properties	A large radius of the nanopillars, resulted in high bactericidal properties (Li, 2016)				
Shape	Shape No significant effect of shape on the bactericidal properties was found in our study.		The sharper the nanopatterned structure, the higher the bactericidal properties (Xue et al., 2015)			
			Sharp nanopatterns enhanced the bactericidal effica (Tripathy et al., 2017)		nanced the bactericidal efficacy	
			atement is not true based the finite element model Statement is uncertain based on the finite element model			

The geometrical features width and interspace showed a significant effect on the bactericidal properties of the nanopatterned surface. The width of the nanopatterned surface was variated in combination with a small interspace and a large interspace. In combination with a small interspace, the width did not influence the bactericidal properties of the nanopatterned surface. While in combination with a large interspace, the variation of width did change the bactericidal properties. Our results showed that a nanopatterned surface with a smaller width in combination with a large interspace showed higher bactericidal properties. The smaller the width, the lower the effective contact area of the nanopattern resulting in higher bactericidal

properties (Hizal et al., 2015). Also the bacteria would interact with more interspaces due to the smaller width, resulting in more deformation of the bacteria. This would increase the stretching of the bacterial wall leading to higher bactericidal properties (Li et al., 2016; Xue et al., 2015).

The variation of the interspace of the nanopatterned surface also showed a clear effect on the bactericidal properties. The larger the interspace, the higher the bactericidal properties. Also this geometrical feature involved the effective contact area. The smaller the interspace, the higher the effective contact area. Resulting in more surface contact of the bacteria with the nanopatterned surface. For the bacteria it was possible to find an equilibrium on top of the nanopatterned surface, like a bed of nails, when the interspace was small. If the interspace was large, the bacteria could not find an equilibrium anymore and the nanopillars would puncture into the bacterial wall (Bandara et al., 2017). This effect is much stronger for the nanopatterned surfaces with a large interspace in combination with a small width than for the nanopatterned surfaces with a large interspace in combination with a large width. Again, this is due to the smaller effective contact area, resulting in a deformation of the bacterial cell on the outer sides of the nanopillars.

The intervariability between width and interspace was statistically tested. The relation between the ratio $\frac{W}{W+IS}$ and the maximum strain in the bacterial wall has been described. The ratio $\frac{W}{W+IS}$ significantly influenced the bactericidal properties. A small ratio was equal to a small width and a large interspace, leading both to a smaller effective surface area and higher bactericidal properties. Also the ratio between the radius and the interspace $\frac{R}{LS}$ showed a significantly effect on the bactericidal properties. A smaller ratio led to higher bactericidal properties, so a smaller radius and a larger interspace of the nanopillars would lead to higher bactericidal properties. The study of Ivanova et al. (2013) stated that the high aspect ratio of the nanostructures contributed to the bactericidal properties of the nanopatterned surface. The aspect ratio was described as the ratio of the height of the nanostructure to the width of the nanostructure (Frazier and Allen, 1992). A high aspect ratio could be reached by increasing the height or by reducing the width of the nanostructures. Our study showed that a smaller width resulted in higher bactericidal properties and a larger height did not influence the bactericidal properties. Therefore, the effect of the ratio's explained before ($\frac{W}{W+IS}$ and $\frac{R}{IS}$), including the width, interspace, and radius could result in a more significant effect of the bactericidal properties than the effect of the aspect ratio.

The maximum strain in the bacterial wall of the osteoblast cell was larger when the interspace increased and the width decreased. The maximum strain in the bacterial wall was higher for the osteoblast cell than for the bacterial cell. Due to the material properties of the osteoblast cell, the osteoblast behaved similarly to the bacterial cell. The higher strain in the cell wall of the osteoblast was due to the lower Young's modulus of the cell wall. However, the stresses in the cell wall of the osteoblast cell were lower than in the bacterial wall. The lower stress in the cell wall of the osteoblast was due to the larger surface area of the osteoblast, which was almost 40 times bigger. The stress could be calculated by dividing the force over the surface area (Bidez and Misch, 2014). So a larger surface area of the osteoblast cell resulted in a lower stress in the cell wall.

The width and the interspace of the nanopatterned surface have the highest influence on the bacterial properties. Figure 26 represents a schedule which shows the bactericidal, non-

bactericidal, cytotoxic and non-cytotoxic properties of the nanopatterned surface based on width and interspace. The nanopatterned surface with an interspace of 300 nm and a width of 25 or 50 nm showed both bactericidal properties. The nanopatterned surfaces with a width larger than 120 showed no bactericidal properties. Also the nanopatterned surfaces with an interspace lower than 100 nm showed no bactericidal properties. The nanopatterned surface with an interspace of 300 nm and a width of 25 nm showed both bactericidal and cytotoxic properties. The only nanopatterned surface resulting in bactericidal properties and non-cytotoxic properties was the nanopatterned surface with an interspace of 300 nm and a width of 50 nm. This nanopatterned surface could be considered as the most optimal nanopattern regarding the geometrical features to kill bacterial cells, while being non-harmful to host cells.

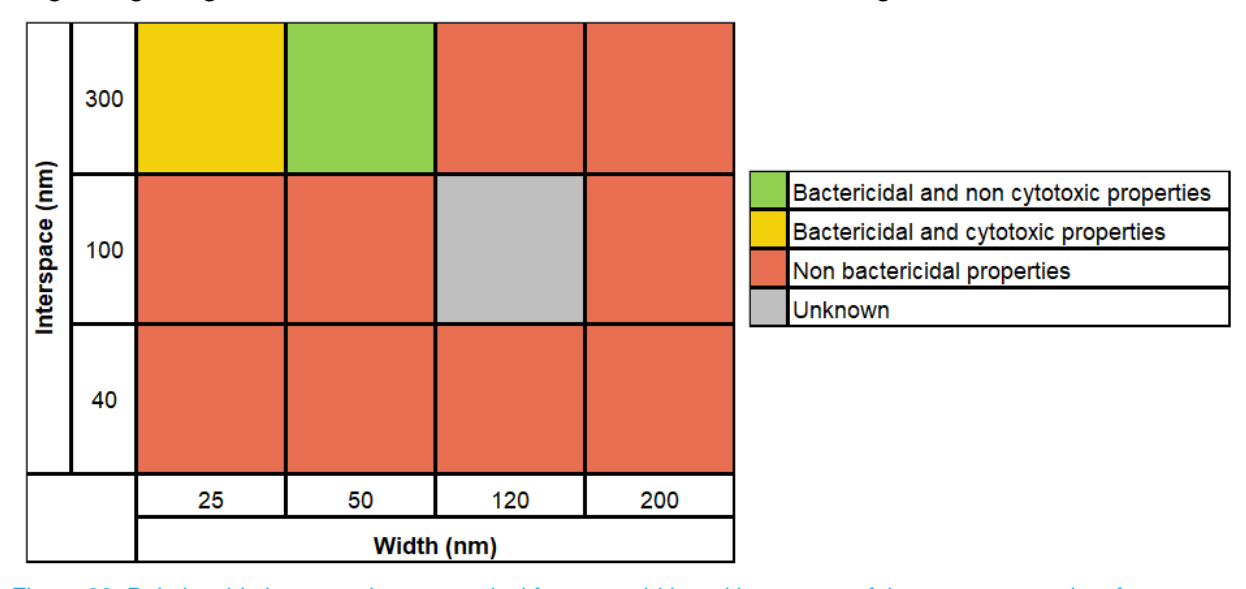


Figure 26: Relationship between the geometrical features width and interspace of the nanopatterned surface regarding the bactericidal and cytotoxic properties.

4.2 Suggestion for the improvement of the FE simulations

4.2.1 Difficulties of the FE simulation

Some issues with respect to convergence occurred during the simulations with the sharp nanopillars. A computational error occurred due to the small contact surface of the nanopatterned surface of type 22. This computational error was solved by using Mooney-Rivlin coefficients instead of Neo-Hookean coefficients as properties for the cytoplasm for one simulation. To make sure the Mooney-Rivlin coefficients did not differ in outcome parameters with respect to the Neo-Hookean coefficients, an analysis comparing Mooney-Rivlin with Neo-Hookean coefficients was made. This analysis compared the nanopatterned surface of type 7, while using Mooney-Rivlin coefficients in one simulation and Neo-Hookean coefficients in another one. The difference in the outcome parameter was less than 1%. Based on the low error percentage, the results of the simulation using the Mooney-Rivlin coefficients could be included. In the supplementary information (S5) the comparison of the Neo-Hookean and Mooney-Rivlin coefficients is given.

4.2. Potential validation of the model

Comparing the outcome parameters of the FE model to already known experimental and analytical outcomes in the literature, could contribute to the validation of the model (Bhadra et al., 2015; Dickson et al., 2015; Hasan et al., 2015; Xue et al., 2015). In the study of Hasan et

al. (2015) nanopillars were fabricated with a width of 220 nm in combination with a random interspacing. These nanopillars showed a bactericidal effect and a cytotoxic effect to host cells. In our study a nanopattern with a width of 200 nm resulted in a non-bactericidal effect and a non-cytotoxic effect, showing the opposite effect of the study of Hasan et al. (2015). Bhadra et al. (2015) created nanowires with a width of 30 nm, a height of 40 nm and a random interspacing. Selective bactericidal properties were shown in this study. Confirming our results that a small width (25 nm - 50 nm) resulted in bactericidal properties. However the interspace was random in the study of Bhadra et al. (2015), which could lead to the selective bactericidal properties of the nanopattern. In the study of Dickson et al. (2015) two different types of nanopillars were fabricated. The type of nanopillars with the smallest width (70 nm) in combination with the smallest interspace (100 nm) resulted in a bactericidal effect. The nanopattern with the largest interspace (380 nm) in combination with a width of 215 nm resulted as well into bactericidal properties. Our findings indicated that the combination of a small width and a large interspace resulted in bactericidal properties. However, in the study of Dickson et al. (2015) a nanopatterned surface with only a small width and only a large interspace resulted in bactericidal properties. Also the sinking depth of the bacteria was observed (Xue et al., 2015). In the model of Xue et al. (2015) the sinking depth of the bacteria ranged from 5 nm to 35 nm. The sinking depth of the bacteria in our model variated between 4 and 30 nm, corresponding to the findings of Xue et al. (2015).

The contradictions between our results and the findings of the study of Hasan et al. (2015) and Dickson et al. (2015) could be due to the computational characteristic of this study. Our simulations only included the physical and mechanical properties of the cells. However the biological properties were not taken into account. Bacteria adhered on the biomaterial surface based on the adhesions on the bacterial wall which made bridges with the biomaterial (Katsikogianni and Missirlis, 2004). Furthermore, environmental factors such as bactericidal concentration and flow rate could influence the behaviour of the bacterial cell as well (Crawford et al., 2012). In our simulations the bacteria always adhered on the nanopatterned surface and only the bactericidal mechanism of the nanopattern was examined. The inclusion of the biological processes into the computational model could help to reduce the difference found between the findings in the study of Hasan et al. (2015) and Dickson et al. (2015) and our results.

The current strain criterion used to determine the bactericidal threshold and the cytotoxic threshold for osteoblast cells could be experimentally validated. The rupture threshold for the cell wall of Staphylococcus aureus is based on an artificial bacterial thread, which represents a gram-positive bacteria (Thwaites and Mendelson, 1985). The rupture threshold for the cell wall of the osteoblast cell is based on the cell wall of another host cell in the human body (Li et al., 2013). Both criteria were based on an approximation of their own cell mechanics, resulting in some uncertainty of the authenticity of both rupture criteria. The validation of the model could determine a threshold criteria for the rupture of the cell wall of Staphylococcus aureus and osteoblast cells which could be compared with the threshold criteria for the rupture of Staphylococcus aureus and osteoblast cells found in literature (Li et al., 2013; Thwaites and Mendelson, 1985).

4.2.3 Future research

4.2.3.1 Experimentally validation of the FE model

Already an attempt was made to validate the model based on comparison with other literature and models. Although the best way to validate the model was to experimentally test all the nanopatterned surfaces of our simulations. A comparison could be made between

nanopatterns based on the experimental results and the computational results. The nanopatterns belonging to a low maximum strain in the bacterial wall should be non-bactericidal in the experimental tests. The nanopatterns belonging to a high maximum strain in the bacterial wall should be bactericidal in the experimental tests. The threshold criterion for the bacterial wall should be in the range between the highest maximum strain of the nanopattern resulting in non-bactericidal properties and the lowest maximum strain of the nanopattern resulting in bactericidal properties. The same comparison could be made to validate the simulation of the interaction of the nanopatterned surface with the osteoblast cell. However, only four simulations were performed for the osteoblast cell making the validation not conclusive.

4.2.3.2 Increasing the complexity of the FE model

The created FE model simulated the interaction between the cells and the nanopatterned surface on a fundamental level. By increasing the complexity of the FE model, the accuracy of the outcome parameters could become higher. In our model the bacterial cell is modelled into two parts: cytoplasm and cell wall, and the osteoblast cell is modelled into three parts: nucleus, cytoplasm and cell wall. The complexity of the model could be increased by increasing the number of modelled parts of the cells. It is important to examine whether a new created part, results in a change of the results. For instance, adding the cell wall to the bacterial cell resulted in a change of more than 20 percent in the average stress of the pillar (S4). If the outcome parameters would not change by adding a new part, then it is unnecessary to increase the complexity and the computational time of the model.

Another adaptation of the model could be based on the material properties. The bacterial wall of the FE model possesses elastic properties (Xue et al., 2015). However, some articles stated that the bacterial wall possesses viscoelastic properties as well (Bailey et al., 2014). Dependent on the viscoelastic coefficients belonging to the bacterial wall, the results of the model could change. The Young's modulus for the bacterial wall ranged from values on the scale of kilopascals to values on the scale of gigapascals (Eaton et al., 2008; Xue et al., 2015). This large range could be due to the differentiation stage of the cell (Dellatore et al., 2008). Also the environmental factors could influence the Young's modulus of the cell (Thwaites and Mendelson, 1985). Both cell walls in our models possess a Young's modulus and a Poisson's ratio based on analytical and computational models (Wang and Xian, 2016; Xue et al., 2015). The variations in material properties showed that it remains difficult to determine the material properties of the bacterial cell and osteoblast cell. A thorough literature study about the material properties of living cells could contribute to more funded material properties for the FE model.

The FE model mimics the experimental test to determine the bacterial activity and cytotoxicity of host cells based on the interaction of the nanopatterned surface with bacteria or host cells. During these experimental tests the nanopattern was put into a culture well plate. A solution of medium with dissolved bacterial cells or host cells was disposed on top of the nanopatterned surface (Hasan et al., 2015). The FE model simulated one bacterial cell adhering to the nanopattern. In the experimental setting never one bacteria adhered to the nanopatterned surface. Always more bacteria would adhere to the nanopattern. Bacteria even adhered on top of the adhered bacteria due to the high solution of bacteria into the medium (Dickson et al., 2015). Our simulation only took into account the mass of one bacteria and the medium which was above the bacteria. It was not only the gravitational force of the adhering bacteria which deformed the bacteria between the pillars, but also the gravitational force of the bacteria on

top of the adhering bacteria. Therefore, the body force applied on Staphylococcus aureus in the FE model could be underestimated. This counts as well for the osteoblast cell.

Bacteria adhering on top of each other on the nanopatterned surface could probably explain as well why nanopatterned surfaces showed partial bactericidal properties in several studies (Diu et al., 2014; Hasan et al., 2015). In the study of Diu et al. (2014) 70 – 80% of the bacteria were killed by the nanowired surface. Hasan et al. (2015) showed that 86% of the Staphylococcus aureus were killed by the nanopillared surface. The first layers of adhering bacteria to the nanopatterned surface could be killed by the nanopattern, partly due to the compression of other bacteria. While the bacteria which adhered on the top part of other bacteria will not be compressed by other bacteria and could survive the nanopatterned surface.

4.2.3.3 Another mechanism to describe the mechanism of the nanopatterned surface

The simulations of this study were based on the currently accepted mechanism of the bactericidal activity of nanopillars. The mechanism was based on the deformation of bacteria between the nanopillars, causing a high stretching degree, resulting in the puncturing of the bacterial wall by the nanopatterned surface (Ivanova et al., 2012; Pogodin et al., 2013). However, Bandara et al. (2017) proposed a new mechanism, based on the strong adhesive force between bacteria and the nanopatterned surface in combination with a shear force when bacteria move away from the nanopatterned surface (Figure 27). The strong adhesive force is based on the secreted extracellular polymeric substances layer, by which the bacteria adheres to the nanopatterned surface. The shear force occurs when the bacteria moves away and causes separation of the inner-cell wall from the outer-cell wall, resulting in bacterial damage (Bandara et al., 2017). This mechanism is proposed for nanopatterned surfaces which differ in height (Figure 27a). However, our simulation showed for each nanopatterned surface an equal height of the nanopillars. This new proposed mechanistic model could be used to test the intervariability between the geometrical features of the nanopatterned surface.

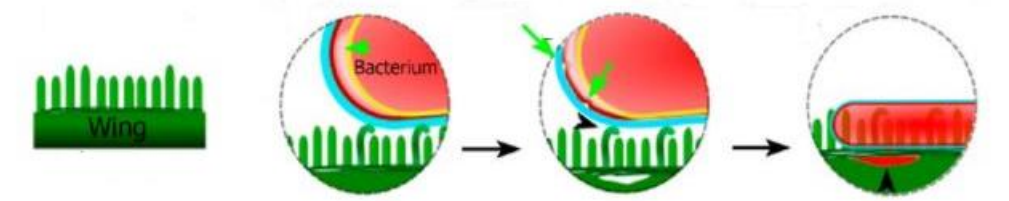


Figure 27: New mechanism for the bactericidal activity of nanopillars. a) Nanopatterned surface with different height of the nanopillars. b) Taller bacteria are bent by the bacteria. The bacteria adheres to the nanopatterned surface by the EPS layer. c) The bacteria tries to move away from the nanopatterned surface. d) Apoptosis of the bacteria and the cytosol leaks out of the bacteria.

4.2.3.4 Elaboration of the concept of nanopatterned surface to other research fields

The concept of nanopatterning of a (bio)material is not only applicable to the orthopaedic field. Also in other medical disciplines it could be used, often in areas where bacteria are causing infections. For instance, stents implemented in the human body often cause infection as a complication. (Ducasse et al., 2004). But also other medical devices still lead to infections (Waldvogel and Bisno, 2000). The fabrication of nanopatterned surfaces on these medical devices could prevent infections in a lot of disciplines of medicine. Besides medicine, every material design which suffers from the accumulation of bacteria could benefit from nanopatterned surfacing. Water treatment processes often encounter biofouling on their membrane filtrations. Causing problems in the performance and the lifetime of the membrane filters (Mansouri et al., 2010). Also the feature of increasing the surface area of the material due to the fabrication of a nanostructures could be beneficial in other material designs. The

nanopatterning on solar cells resulted in an increased efficiency of harvesting light, due to the increased surface area (Kim et al., 2012). This study showed the bactericidal mechanism of the nanopatterning on the implants surface. However, the promising features of nanopatterning can be beneficial in many other fields, such as: other medical devices, water treatment processes and solar cells.

5. Conclusion

Nanopatterned surfaces with different geometrical features were analysed. Based on an FE model the bactericidal and cytotoxic properties of these nanopatterns were examined. Variations in the width and interspace showed significantly the largest effect on the bactericidal properties. The radius showed a smaller significant effect on the bactericidal properties. While the height and shape did not show a significant effect on the bactericidal properties. It was found that two tested nanopatterns lead to the killing of the bacterial cell. Both nanopatterns with bactericidal properties had an interspace of 300 nm, while one was combined with a width of 25 nm and the other one with a width of 50 nm. Only the nanopatterned surface with an interspace of 300 nm in combination with a width of 50 nm resulted in non-cytotoxicity of host cells. The most promising outcome of this study is the confirmation of the bactericidal properties of nanopatterned surfaces based on a FE model. The bactericidal surface might help to lower the infection problem at the surface of the implant. In combination with the cytotoxic tests for host cells a recommendation for the most effective nanopattern was found. The nanopatterned surface with an interspace of 300 nm and a width of 50 nm is proposed as the nanopattern with the most optimum geometrical features resulting in the highest bactericidal properties combined with non-cytotoxicity to host cells.

6. Supplementary information

6.1 Analysis of the time period

The bacterial cell and the osteoblast cell consisted of viscoelastic and elastic properties. Viscoelastic properties possessed a time dependent characteristic. A constant load was applied on both cells, resulting in a time dependent deformation, which was called creep. Prony series were used to relate relaxation and creep functions to viscoelastic materials (Pacheco et al., 2015). Tau, a coefficient of the prony series, represented the relaxation time constant. A multiplication of tau was implemented for the time period. It was important the viscous material had sufficient time to deform. Therefore multiple multiplications of tau were implemented as time period to examine which time period offered enough time for the model to fully adapt. In Figure S1, five different time periods were analysed. The chosen time period was 187.5 seconds, which had a multiplication factor of 10 with tau. The error based on the average stress of the pillars was less than 1% for time periods which were longer than 187.5 seconds. The small error percentage showed that the viscoelastic material was fully deformed at 187.5 seconds (Zhou et al., 2005).

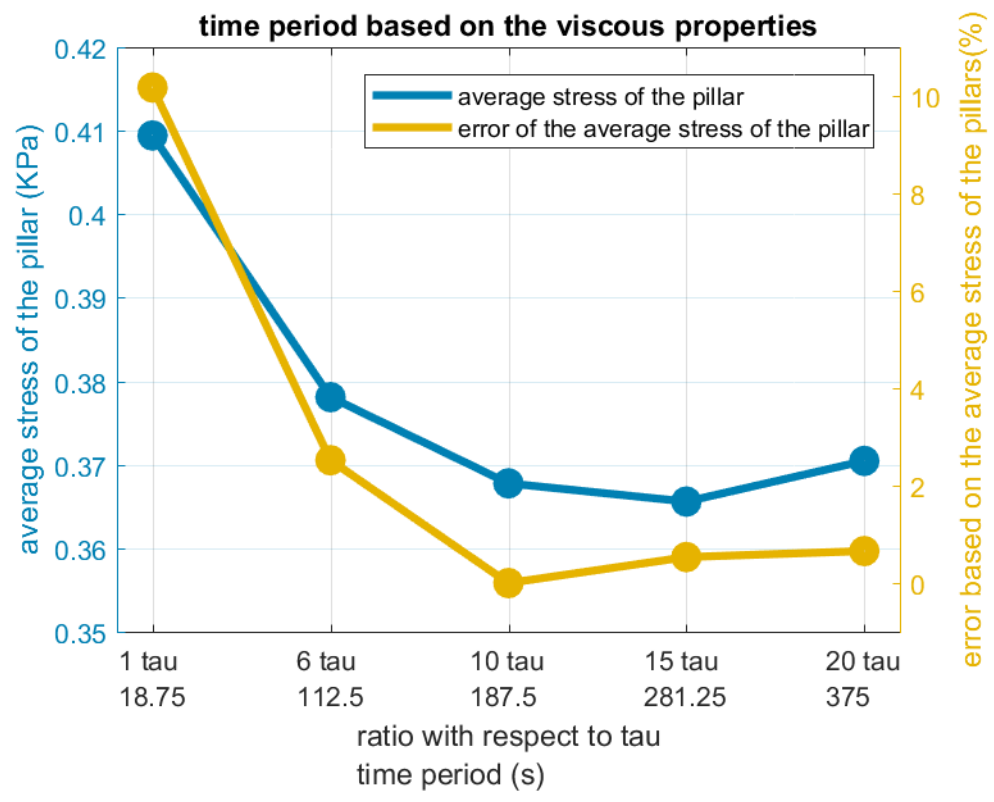


Figure S1: Analysis of the time period.

6.2 Analysis of the ratio of the Young's modulus

A large difference existed between the Young's modulus of the bacterial wall and the nanopatterned surface. The Young's modulus of the bacterial wall was 6 KPa and the Young's modulus of the nanopatterned surface was 150 GPa. The Young's modulus of the nanopatterned surface was 25 million times bigger.

The Young's modulus of the nanopatterned surface was decreased to 150 MPA and to 1.5 MPa to examine whether the large difference between the Young's modulus influenced the results. Decreasing the Young's modulus of the nanopatterned surface with a factor 100.000, resulted in an error percentage less than 0.2% based on the average stress in the pillar. This error percentage was negligible. The large difference between the Young's modulus of the bacterial wall and the nanopatterned surface did not influence the results.

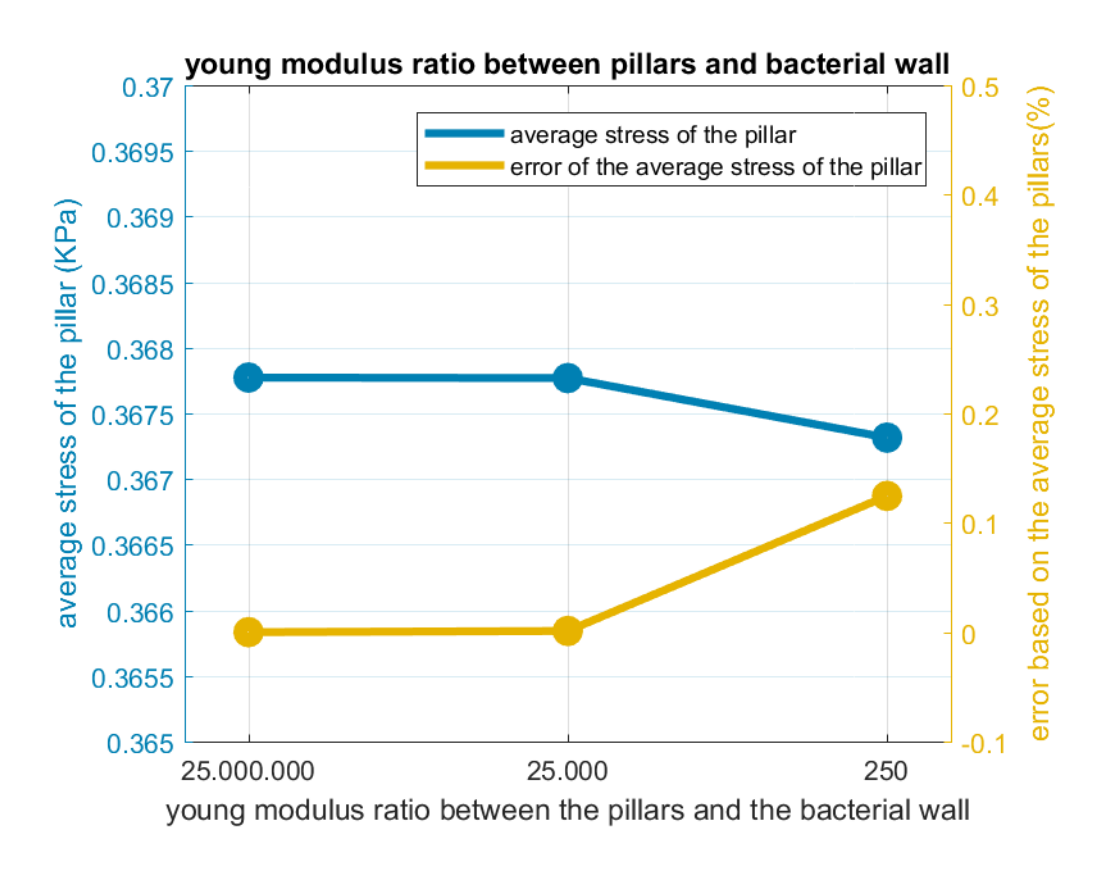


Figure S2: Analysis of the difference in Young's modulus of the nanopatterned surface and the bacterial wall.

6.3 Mesh refinement

6.3.1 Meshing of Staphylococcus aureus

For the analysis with the bacterial cell, twenty-two different models were created. As a reference model for the mesh refinement the model with the smallest nanopillars was chosen. When the solution converged for the model with the smallest nanopillars, it would converge for models with larger nanopillars as well. Four different mesh sizes were chosen. The interspaces between adjacent nodes were 5.25 nm, 4 nm, 3 nm and 1.95 nm. In Figure S3 the error percentage of the average stress of the pillars is illustrated. The chosen mesh size had an interspace of 3 nm between adjacent nodes. The error percentage of the model with a mesh size of 1.95 nm between adjacent nodes was less than 0.5%. The computational time of the model with a mesh size of 1.95 nm was more than 3 times as much as the computational time of the model with a mesh size of 3 nm. Considering the small error percentage and a high increase in computational time, the reference mesh size of the models was 3 nm. Figure S4 shows the mesh of Staphylococcus aureus with a mesh size of 3 nm.

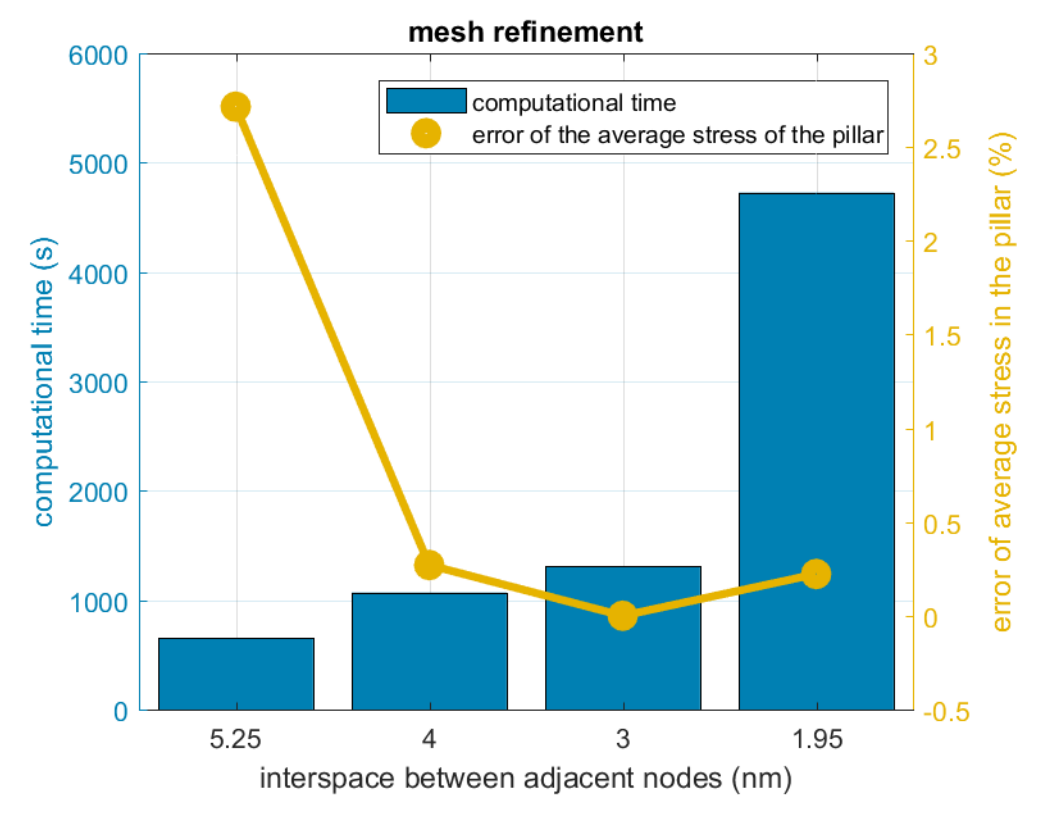


Figure S3: Mesh refinement for the reference model of the interaction between nanopatterned surfaces and Staphylococcus aureus.

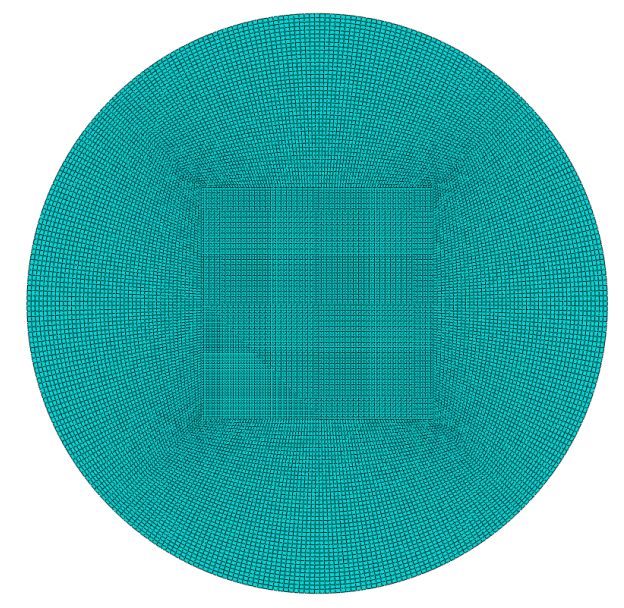


Figure S4: Mesh of Staphylococcus aureus with a mesh size of 3 nm.

6.3.2 Meshing of the osteoblast cell

For the analysis with the osteoblast cell, four different models were created. The model with the smallest nanopillars was chosen as a reference model, with the same reason as for the bacterial cell. Four different mesh sizes were chosen. The interspaces between adjacent nodes were 14 nm, 12 nm, 10 nm and 6.5 nm. In Figure S5 the error percentage of the average stress in the cell wall of the osteoblast is illustrated. The chosen mesh size had an interspace

of 10 nm between adjacent nodes. The error percentage of the model with a mesh size of 6.5 nm was less than 1% in comparison with the mesh size of 10 nm. Only few simulations were performed for the osteoblast cell, therefor the computational time was less important. Considering the small error percentage, the reference element size of the model was 10 nm. Figure S6 shows the mesh of the osteoblast cell with the mesh size of 10 nm.

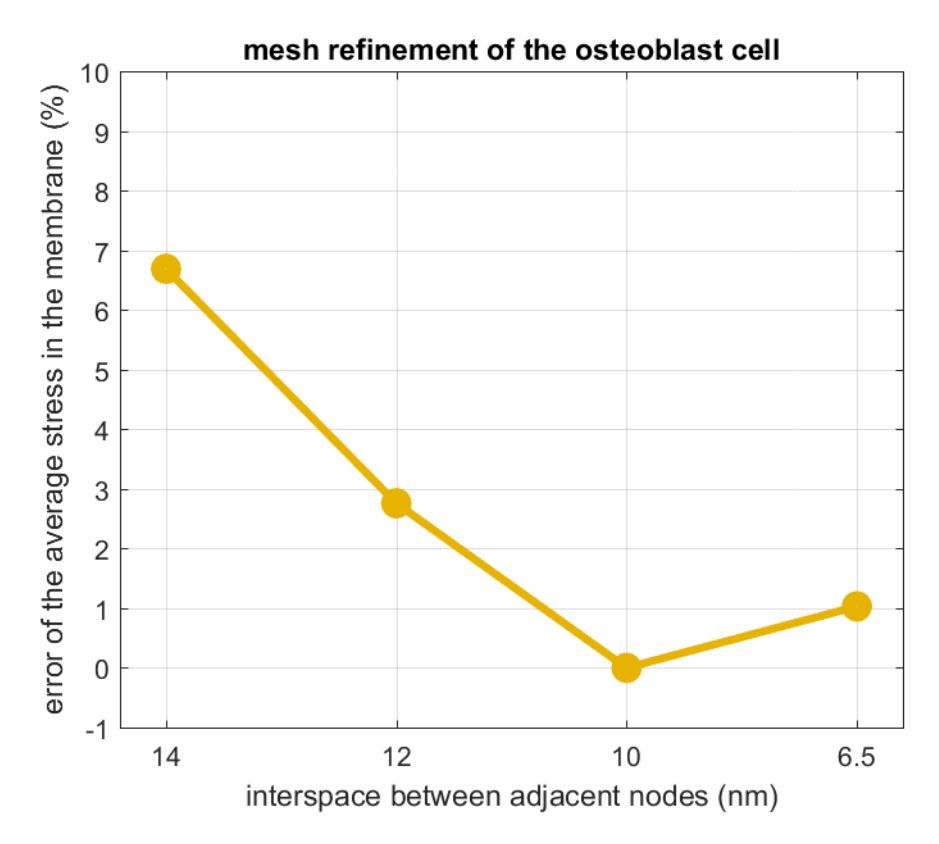


Figure S5: Mesh refinement for the reference model of the interaction between nanopatterned surfaces and the osteoblast cell.

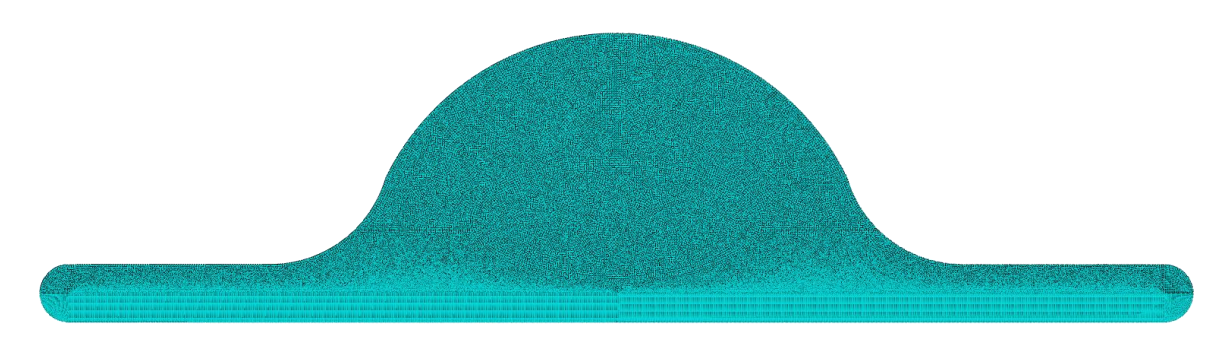


Figure S6: Mesh of the osteoblast cell with a mesh size of 10 nm.

6.4 Interaction between the cytoplasm and the cell wall of Staphylococcus aureus

For the calculations of the body force, it is necessary to know the mass of Staphylococcus aureus. The mass of Staphylococcus aureus was 1 pg. The calculations of the body force were performed at the subsection 'loading, boundary conditions and interaction'. In our simulations the mass distribution between the bacterial wall and the cytoplasm was 50%-50%. It was compared to a mass distribution of 20% cytoplasm, 80% cell wall and a mass distribution of

80% cytoplasm, 20% cell wall. The error based on the average stress in the pillars was less than 1% (Figure S7). Indicating that the mass distribution almost did not influence the results. Another simulation was performed where only the bacterial cell was described based on only cytoplasm and no cell wall. The error percentage of the average stress was more than 20%, between the simulations of the bacterial cell with and without a cell wall. The bacterial wall did influence the results and therefore should be modelled.

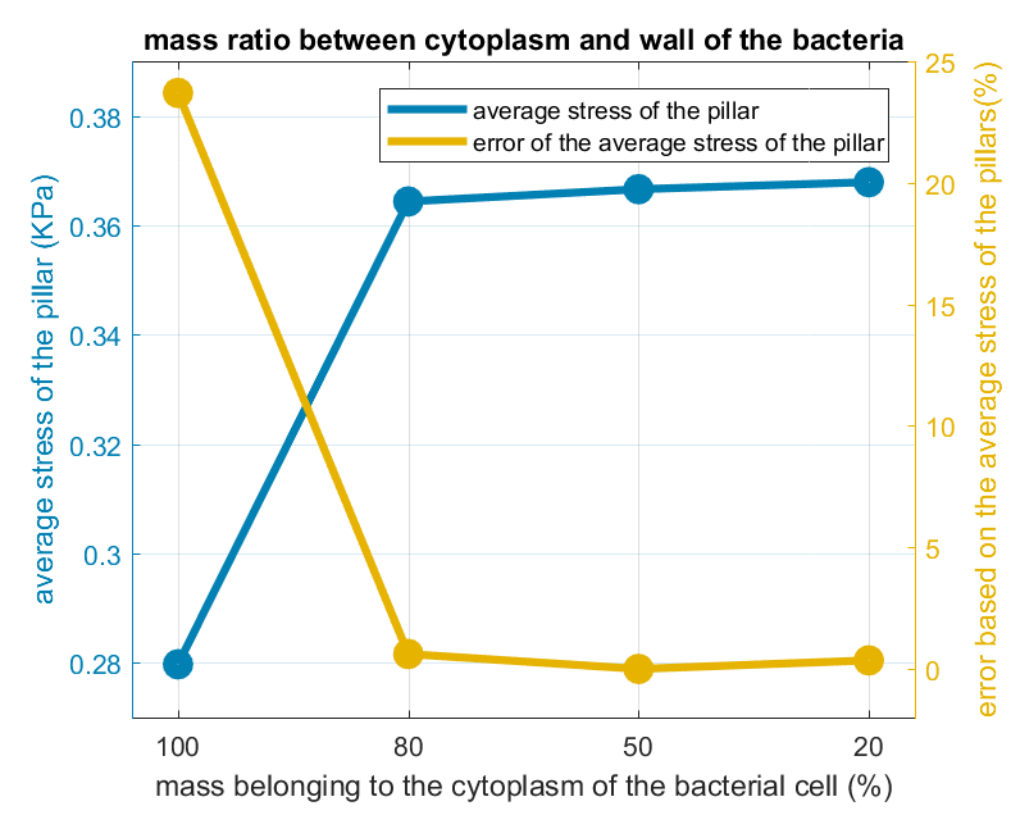


Figure S7: Mass ratio analysis between the cytoplasm and the cell wall of Staphylococcus aureus.

6.5 Analysis of the hyperelastic coefficients

Simulation type 22 did not finish due to computational errors. Reducing the mesh size and changing the distance between the nanopatterned surface and the bacteria did not help to solve the computational errors. Therefore other hyperelastic coefficients were used to solve the problem. Mooney-Rivlin coefficients existed as one of the first models to describe hyperelastic models (Martins et al., 2006). The difference between the chosen Neo-Hookean hyperelastic coefficients and the Mooney-Rivlin coefficients was that Neo-Hookean had only 2 coefficients (C_{10} and D_{1}) and Mooney-Rivlin had 3 coefficients (C_{1} , C_{10} and D_{1}). For the Neo-Hookean coefficients C_{1} was set at 0 (Shahzad et al., 2015). The calculation of the Mooney-Rivlin coefficients could be performed using the following formulas (Felhos et al., 2008):

$$E = 6 \left(C_{10} + C_{01} \right) \tag{12}$$

$$4 = \frac{C_{10}}{C_{01}} \tag{13}$$

Implementing the Mooney-Rivlin coefficients ($C_{01} = 1.2*10^{-5}$ and $C_{10} = 4.8*10^{-5}$) into simulation type 22 solved the problem. Both coefficients resembled the hyperelastic behaviour, however

the solution could deviate from the other because another type of coefficients was used. Therefore, a simulation which was already finished with Neo-Hookean coefficients (Type 7) was tested with Mooney-Rivlin coefficients as well. The error percentage based on the average stress in the pillar, the maximum strain in the bacterial wall and the maximum stress in the bacterial wall was less than 1%. The error percentage based on the sinking depth ratio was 1.18% (Figure S8). These results illustrated that the Mooney-Rivlin coefficients gave a low error percentage. Therefore simulation type 22 with the implementation of Mooney-Rivlin coefficients could be included in the results and could be compared with the other simulations.

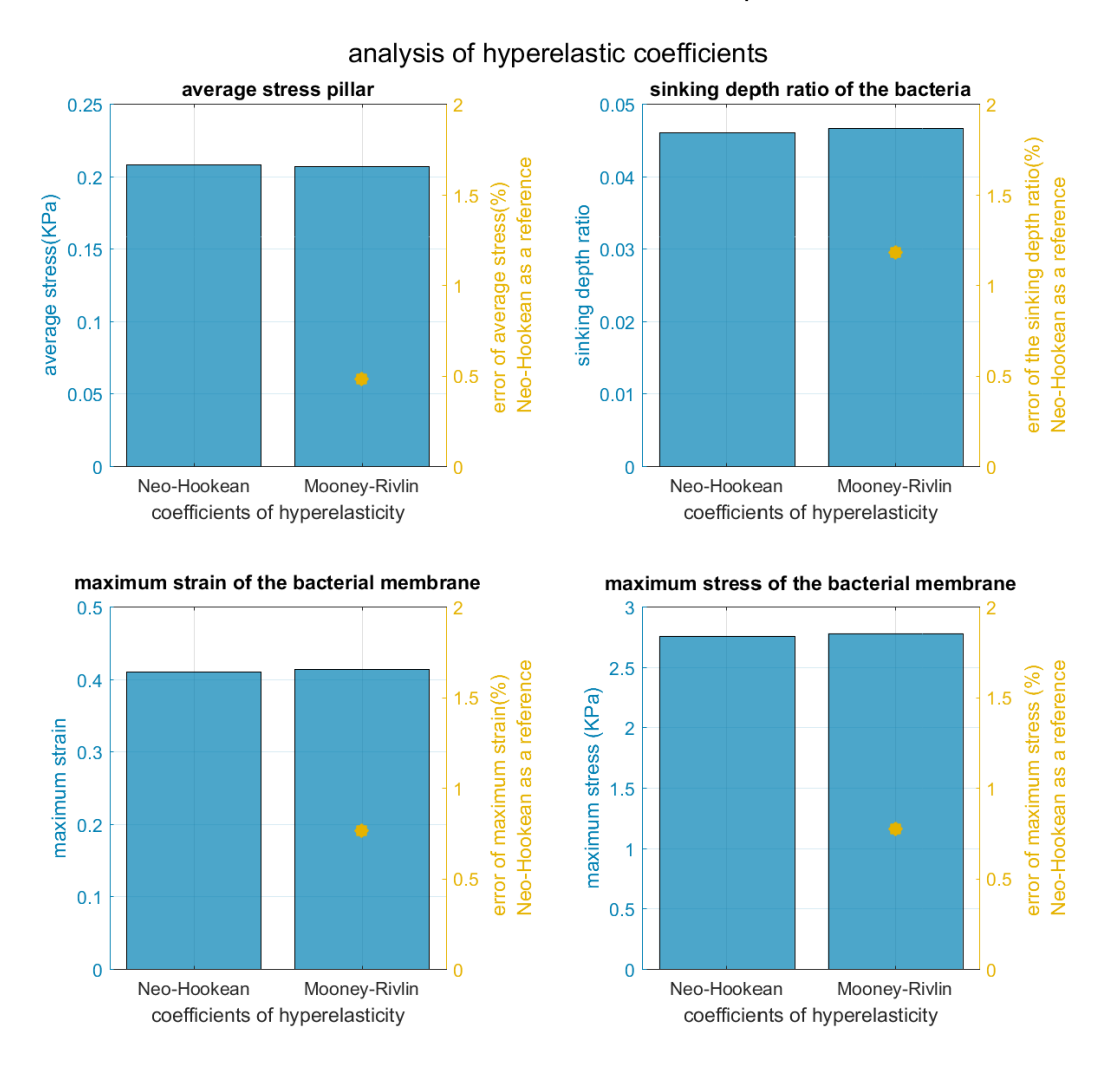


Figure S8: Analysis for comparison between Neo-Hookean coefficients and Mooney-Rivlin coefficients.

7. Bibliography

- Bailey, R. G., Turner, R. D., Mullin, N., Clarke, N., Foster, S. J., & Hobbs, J. K. (2014). The interplay between cell wall mechanical properties and the cell cycle in Staphylococcus aureus. *Biophysical journal*, *107*(11), 2538-2545.
- Bandara, C. D., Singh, S., Afara, I. O., Tesfamichael, T., Wolff, A., Ostrikov, K., & Oloyede, A. (2017). Bactericidal Effects of Natural Nanotopography of Dragonfly Wing on Escherichia coli. *ACS applied materials & interfaces*.
- Bhadra, C. M., Truong, V. K., Pham, V. T., Al Kobaisi, M., Seniutinas, G., Wang, J. Y., . . . Ivanova, E. P. (2015). Antibacterial titanium nano-patterned arrays inspired by dragonfly wings. *Scientific reports, 5*, 16817.
- Bidez, M. W., & Misch, C. E. (2014). Clinical biomechanics in implant dentistry. *Dental Implant Prosthetics-E-Book*, 95.
- Campoccia, D., Montanaro, L., & Arciola, C. R. (2006). The significance of infection related to orthopedic devices and issues of antibiotic resistance. *Biomaterials*, *27*(11), 2331-2339.
- Cowin, S. C., & Doty, S. B. (2007). Tissue mechanics: Springer Science & Business Media.
- Craig, L. E., Dittmer, K. E., & Thompson, K. G. (2015). Bones and joints. *Jubb, Kennedy, and Palmer's Pathology of Domestic Animals*, *1*, 16-163.
- Crawford, R. J., Webb, H. K., Truong, V. K., Hasan, J., & Ivanova, E. P. (2012). Surface topographical factors influencing bacterial attachment. *Advances in colloid and interface science*, *179*, 142-149.
- Dellatore, S. M., Garcia, A. S., & Miller, W. M. (2008). Mimicking stem cell niches to increase stem cell expansion. *Current opinion in biotechnology*, *19*(5), 534-540.
- Dickson, M. N., Liang, E. I., Rodriguez, L. A., Vollereaux, N., & Yee, A. F. (2015). Nanopatterned polymer surfaces with bactericidal properties. *Biointerphases, 10*(2), 021010.
- Diu, T., Faruqui, N., Sjöström, T., Lamarre, B., Jenkinson, H. F., Su, B., & Ryadnov, M. G. (2014). Cicada-inspired cell-instructive nanopatterned arrays. *Scientific reports, 4*, 7122.
- Dobbenga, S., Fratila-Apachitei, L. E., & Zadpoor, A. A. (2016). Nanopattern-induced osteogenic differentiation of stem cells—A systematic review. *Acta Biomaterialia*, *46*, 3-14.
- Ducasse, E., Calisti, A., Speziale, F., Rizzo, L., Misuraca, M., & Fiorani, P. (2004). Aortoiliac stent graft infection: current problems and management. *Annals of vascular surgery,* 18(5), 521-526.
- Eaton, P., Fernandes, J. C., Pereira, E., Pintado, M. E., & Malcata, F. X. (2008). Atomic force microscopy study of the antibacterial effects of chitosans on Escherichia coli and Staphylococcus aureus. *Ultramicroscopy*, *108*(10), 1128-1134.
- Elbourne, A., Crawford, R. J., & Ivanova, E. P. (2017). Nano-structured antimicrobial surfaces: From nature to synthetic analogues. *Journal of Colloid and Interface Science*, *508*, 603-616.
- Felhos, D., Xu, D., Schlarb, A., Váradi, K., & Goda, T. (2008). Viscoelastic characterization of an EPDM rubber and finite element simulation of its dry rolling friction. *Express Polymer Letters*, *2*(3), 157-164.
- Francius, G., Domenech, O., Mingeot-Leclercq, M. P., & Dufrêne, Y. F. (2008). Direct observation of Staphylococcus aureus cell wall digestion by lysostaphin. *Journal of bacteriology*, 190(24), 7904-7909.
- Frazier, A. B., & Allen, M. G. (1992). *High aspect ratio electroplated microstructures using a photosensitive polyimide process.* Paper presented at the Micro Electro Mechanical Systems, 1992, MEMS'92, Proceedings. An Investigation of Micro Structures, Sensors, Actuators, Machines and Robot. IEEE.

- Harris, L., Foster, S., & Richards, R. (2002). An introduction to Staphylococcus aureus, and techniques for identifying and quantifying S. aureus adhesins in relation to adhesion to biomaterials: review. *Eur Cell Mater, 4*(3).
- Hartmann, C., Mathmann, K., & Delgado, A. (2006). Mechanical stresses in cellular structures under high hydrostatic pressure. *Innovative food science & emerging technologies*, 7(1), 1-12.
- Hasan, J., Raj, S., Yadav, L., & Chatterjee, K. (2015). Engineering a nanostructured "super surface" with superhydrophobic and superkilling properties. *RSC Advances*, *5*(56), 44953-44959.
- Hizal, F., Zhuk, I., Sukhishvili, S., Busscher, H. J., van der Mei, H. C., & Choi, C.-H. (2015). Impact of 3D hierarchical nanostructures on the antibacterial efficacy of a bacteriatriggered self-defensive antibiotic coating. *ACS applied materials & interfaces, 7*(36), 20304-20313.
- Ivanova, E. P., Hasan, J., Webb, H. K., Gervinskas, G., Juodkazis, S., Truong, V. K., . . . Watson, G. S. (2013). Bactericidal activity of black silicon. *Nature communications, 4*.
- Ivanova, E. P., Hasan, J., Webb, H. K., Truong, V. K., Watson, G. S., Watson, J. A., . . . Tobin, M. J. (2012). Natural bactericidal surfaces: mechanical rupture of Pseudomonas aeruginosa cells by cicada wings. *Small*, *8*(16), 2489-2494.
- Jin, Y., Zhang, Y., Ouyang, H., Peng, M., Zhai, J., & Li, Z. (2015). Quantification of Cell Traction Force of Osteoblast Cells Using Si Nanopillar-Based Mechanical Sensor. *Sensors and Materials*, 27(11), 1071-1077.
- Kapadia, B. H., Berg, R. A., Daley, J. A., Fritz, J., Bhave, A., & Mont, M. A. (2016). Periprosthetic joint infection. *The Lancet, 387*(10016), 386-394.
- Katsikogianni, M., & Missirlis, Y. (2004). Concise review of mechanisms of bacterial adhesion to biomaterials and of techniques used in estimating bacteria-material interactions. *Eur Cell Mater*, 8(3).
- Kelleher, S. M., Habimana, O., Lawler, J., O'Reilly, B., Daniels, S., Casey, E., & Cowley, A. (2015). Cicada wing surface topography: An investigation into the bactericidal properties of nanostructural features. *ACS applied materials & interfaces*, 8(24), 14966-14974.
- Kim, J., Koh, J. K., Kim, B., Kim, J. H., & Kim, E. (2012). Nanopatterning of Mesoporous Inorganic Oxide Films for Efficient Light Harvesting of Dye-Sensitized Solar Cells. *Angewandte Chemie*, 124(28), 6970-6975.
- Kusters, G. A. M., & Hendriks, M. A. N. (1994). DIANA Computational Mechanics. *Kluwer Academic Publisher*, 139-148.
- Li, F., Chan, C. U., & Ohl, C. D. (2013). Yield strength of human erythrocyte membranes to impulsive stretching. *Biophysical journal*, *105*(4), 872-879.
- Li, H., & Lykotrafitis, G. (2014). Erythrocyte membrane model with explicit description of the lipid bilayer and the spectrin network. *Biophysical journal*, *107*(3), 642-653.
- Li, X. (2016). Bactericidal mechanism of nanopatterned surfaces. *Physical Chemistry Chemical Physics*, *18*(2), 1311-1316.
- Lowy, F. D. (1998). Staphylococcus aureus infections. *New England journal of medicine*, 339(8), 520-532.
- Mansouri, J., Harrisson, S., & Chen, V. (2010). Strategies for controlling biofouling in membrane filtration systems: challenges and opportunities. *Journal of Materials Chemistry*, 20(22), 4567-4586.
- Martins, P., Natal Jorge, R., & Ferreira, A. (2006). A comparative study of several material models for prediction of hyperelastic properties: Application to silicone-rubber and soft tissues. *Strain*, *42*(3), 135-147.
- Mavrogenis, A., Dimitriou, R., Parvizi, J., & Babis, G. (2009). Biology of implant osseointegration. *J Musculoskelet Neuronal Interact*, *9*(2), 61-71.
- Milner, J. S., Grol, M. W., Beaucage, K. L., Dixon, S. J., & Holdsworth, D. W. (2012). Finite-element modeling of viscoelastic cells during high-frequency cyclic strain. *Journal of functional biomaterials*, *3*(1), 209-224.

- Pacheco, J. E. L., Bavastri, C. A., & Pereira, J. T. (2015). Viscoelastic relaxation modulus characterization using Prony series. *Latin American Journal of Solids and Structures*, 12(2), 420-445.
- Panagiotopoulou, O., Wilshin, S., Rayfield, E., Shefelbine, S., & Hutchinson, J. (2012). What makes an accurate and reliable subject-specific finite element model? A case study of an elephant femur. *Journal of the Royal Society Interface*, *9*(67), 351-361.
- Perry, J. J., Staley, J. T., & Lory, S. (2002). Microbial life: Sinauer Associates Incorporated.
- Pogodin, S., Hasan, J., Baulin, V. A., Webb, H. K., Truong, V. K., Nguyen, T. H. P., . . . Watson, J. A. (2013). Biophysical model of bacterial cell interactions with nanopatterned cicada wing surfaces. *Biophysical journal*, 104(4), 835-840.
- Shahzad, M., Kamran, A., Siddiqui, M. Z., & Farhan, M. (2015). Mechanical characterization and FE modelling of a hyperelastic material. *Materials Research*, 18(5), 918-924.
- Shockman, G. D., & Barren, J. (1983). Structure, function, and assembly of cell walls of grampositive bacteria. *Annual Reviews in Microbiology*, *37*(1), 501-527.
- Silhavy, T. J., Kahne, D., & Walker, S. (2010). The bacterial cell envelope. *Cold Spring Harbor perspectives in biology*, 2(5), a000414.
- Thwaites, J., & Mendelson, N. H. (1985). Biomechanics of bacterial walls: studies of bacterial thread made from Bacillus subtilis. *Proceedings of the National Academy of Sciences*, 82(7), 2163-2167.
- Trickey, W. R., Lee, G. M., & Guilak, F. (2000). Viscoelastic properties of chondrocytes from normal and osteoarthritic human cartilage. *Journal of Orthopaedic Research, 18*(6), 891-898.
- Tripathy, A., Sen, P., Su, B., & Briscoe, W. H. (2017). Natural and bioinspired nanostructured bactericidal surfaces. *Advances in colloid and interface science*.
- Vincent, W. J. (2005). Statistics in kinesiology (Vol. 10): John Wiley & Sons.
- Waldvogel, F. A., & Bisno, A. L. (2000). *Infections associated with indwelling medical devices*: ASM press Washington, DC.
- Wang, B., & Anslyn, E. V. (2011). *Chemosensors: principles, strategies, and applications* (Vol. 15): John Wiley & Sons.
- Wang, L., Hsu, H.-Y., Li, X., & Xian, C. J. (2016). Effects of Frequency and Acceleration Amplitude on Osteoblast Mechanical Vibration Responses: A Finite Element Study. *BioMed research international*, 2016.
- Wang, L., & Xian, C. J. (2016). Dynamic analyses of osteoblast vibrational responses: a finite element viscoelastic model. *Journal of Vibroengineering*, 18(7).
- Wu, S., Zuber, F., Brugger, J., Maniura-Weber, K., & Ren, Q. (2016). Antibacterial Au nanostructured surfaces. *Nanoscale*, 8(5), 2620-2625.
- Xue, F., Liu, J., Guo, L., Zhang, L., & Li, Q. (2015). Theoretical study on the bactericidal nature of nanopatterned surfaces. *Journal of theoretical biology*, *385*, 1-7.
- Zhou, E., Lim, C., & Quek, S. (2005). Finite element simulation of the micropipette aspiration of a living cell undergoing large viscoelastic deformation. *Mechanics of Advanced Materials and Structures*, *12*(6), 501-512.